# Nature of the active sites in CO oxidation on FeSiBEA zeolites

Ireneusz Kocemba, Jacek Rynkowski, Jacek Gurgul, Robert P. Socha, Kazimierz Łątka, Jean-Marc Krafft, Stanislaw Dzwigaj

# Nature of the active sites in CO oxidation on FeSiBEA zeolites

Ireneusz Kocemba[1], Jacek Rynkowski[1], Jacek Gurgul[2], Robert P. Socha[2], Kazimierz Łątka[3], Jean-Marc Krafft[4,5], Stanislaw Dzwigaj[4,5,*]

[1] Lodz University of Technology, Institute of General and Ecological Chemistry, Żeromskiego 116, 90-924 Łódź, Poland

[2]Jerzy Haber Institute of Catalysis and Surface Chemistry, Polish Academy of Sciences, Niezapominajek 8, 30-239 Kraków, Poland

[3]M. Smoluchowski Institute of Physics, Jagiellonian University, Łojasiewicza 11, 30-348 Kraków, Poland

[4]Sorbonne Universités, UPMC Univ Paris 06, UMR 7197, Laboratoire de Réactivité de Surface, 4 place Jussieu, Case 178, F-75005, Paris, France

[5]CNRS, UMR 7197, Laboratoire de Réactivité de Surface, 4 place Jussieu, Case 178, F-75005, Paris, France

Figures : 15

Tables : 2

Keywords: Fe, zeolite**,** CO, oxidation, Mössbauer

*Corresponding author: Stanislaw Dzwigaj, E-mail: stanislaw.dzwigaj@upmc.fr,

tel: +33 1 44 27 21 13

**Abstract**

FeSiBEA zeolites containing 1 wt % of iron were prepared by a two-step postsynthesis method in acidic (pH = 2.6) ($Fe_{1.0}$SiBEA(w)) and alkaline (pH = 10) ($Fe_{1.0}$SiBEA(p)) conditions. The structure of the studied materials, their acidity as well as the nature and environment of iron present in the samples were studied by means of XRD, FTIR with CO as probe molecule, DR UV–vis, Mössbauer and XPS spectroscopies, respectively. Temperature-Programmed Surface Reaction (TPSR) was used to test the catalytic activity of FeSiBEA zeolites in CO oxidation in air in the temperature range of 298–773 K. It was shown that $Fe_{1.0}$SiBEA(w) contains iron as framework pseudo-tetrahedral Fe(III), in contrast to $Fe_{1.0}$SiBEA(p), in which additional octahedral $FeO_x$ oligomers were identified. Moreover, the presence of two kinds of pseudo-tetrahedral Fe(III) sites with different distortion was distinguished in $Fe_{1.0}$SiBEA(w). The higher catalytic activity was showed by $Fe_{1.0}$SiBEA(w) zeolite containing iron as a strongly distorted pseudo-tetrahedral Fe(III) well dispersed in the framework of SiBEA zeolite. The model of probable active iron centre in $Fe_{1.0}$SiBEA(w) was presented.

## 1. Introduction

The oxidation of CO is one of the most studied heterogeneous catalytic reaction. This reaction is relatively simple and may serve as a model in order to understand the mechanism of reaction on a given catalyst. Moreover, the removal of CO is important in the control of air pollution, vehicle exhaust emission and some industrial processes. So far, some oxides such as hopcalite and supported noble metal catalysts are known to oxidize CO at ambient temperature [1-4]. Recently, some attempts were made to elaborate a new type of catalysts without noble metals [5,6].

The unique physicochemical properties of zeolites have made them a very promising class of materials for various catalytic applications. Zeolites containing iron are active in numerous reactions, including decomposition of nitrogen oxides, selective catalytic reduction of NO with hydrocarbons, benzene oxidation or CO oxidation [7-10]. Nevertheless, the nature of the active sites in zeolites containing iron is still a matter of discussion [11–13].

In our previous paper [14], we have showed that the catalytic activity of $Fe_x$SiBEA in the oxidation of CO strongly depends on the content of iron in the SiBEA structure. We have clearly demonstrated that with increase of iron content above 1 wt % the catalytic activity of $Fe_x$SiBEA starts to decrease significantly. It seems that such properties of $Fe_x$SiBEA are related to the change of the state of iron in this catalyst with increasing of the iron content. As it was shown earlier [14,15], $Fe_x$SiBEA catalyst with low iron content (lower than 1 wt %), contains iron mainly in the form of homogeneously distributed pseudo-tetrahedral Fe(III) present as framework T-atom sites. In contrast, in $Fe_x$SiBEA catalyst with higher iron content (higher than 1 wt %) besides of pseudo-tetrahedral Fe (III), also extra-framework $FeO_x$ oligomers and superparamagnetic Fe-oxyhydroxide were present. Thus, the observed higher activity of $Fe_x$SiBEA catalysts with low iron content may be attributed to the presence of well dispersed pseudo-tetrahedral Fe(III) in the zeolite framework.

However, framework pseudo-tetrahedral Fe(III) are coordinatively saturated and therefore not able to adsorb CO or $O_2$, in line with earlier work on Fe-containing zeolites [15,16]. As we have announced in our earlier work [14], more detailed investigations attempting to identify the adsorption sites responsible for their catalytic activity were undertaken.

The purpose of this study was to well discribe of the nature of iron incorporated into the framework of SiBEA zeolite active in CO oxidation over Fe-zeolite system.

## 2. Experimental

### 2.1. Samples preparation

The FeSiBEA catalyst containing 1 wt % of Fe was prepared by the two-step postsynthesis method described earlier [14]. In the first step, a tetraethylammonium beta (TEABEA) zeolite (Si/Al = 11) from RIPP (China) was dealuminated by its treatment with a 13 mol $L^{-1}$ $HNO_3$ solution for 4 h at 353 K under stirring. The resulting dealuminated SiBEA zeolite (Si/Al > 1300) with vacant T-atom sites was recovered by centrifugation, washed with distilled water and dried overnight at 353 K.

The obtained white SiBEA powder was divided into two parts**.** Then Fe ions were introduced into vacant T-atom sites of SiBEA zeolite by its impregnation in air with $0.6 \times 10^{-2}$ mol $L^{-1}$ aqueous $Fe(NO_3)_3 \cdot 9\ H_2O$ solution. In order to obtain samples with different chemical states of iron in the zeolite structure, but with identical Fe loading, the process of impregnation was carried out under various pH conditions. The first portion of dealuminated SiBEA was impregnated at pH = 2.6 and the second one at pH = 10. After drying in air at 353 K for 24 h the sample obtained at pH=2.6 was white, while that obtained at pH = 10 was pink and were labelled $Fe_{1.0}$SiBEA(w) and $Fe_{1.0}$SiBEA(p), respectively. These samples were further calcined at 773 K for 3 h in air and labelled C-$Fe_{1.0}$SiBEA(w) and C-$Fe_{1.0}$SiBEA(p),

respectively. A detailed description of the method of samples preparation can be found in our earlier work [14].

The main objective of this study was to understand the catalytic activity of $Fe_{1.0}$SiBEA(w) as a function of its preparation condition. Thus, the white $Fe_{1.0}$SiBEA(w) zeolite catalyst prepared in particular condition (pH = 2.6, concentration of Fe precursor $10^{-3}$ mol $L^{-1}$) by two-step postsynthesis method was well characterised using different physico-chemical techniques ($S_{BET}$ = 710 $m^2$ $g^{-1}$ and micropores volume of 0.24 mL $g^{-1}$). In addition, for comparison, also another pink $Fe_{1.0}$SiBEA(p) zeolite catalyst were prepared at pH = 10 ($S_{BET}$ = 700 $m^2$ $g^{-1}$ and micropores volume of 0.24 mL $g^{-1}$) as well as brown 1%Fe/$SiO_2$ catalyst were used in this work as reference. The latter one was prepared by wet impregnation of $SiO_2$ ($S_{BET}$ = 394 $m^2$/g, granular 60-80 mesh) with aqueous $Fe(NO_3)_3 \cdot 9H_2O$ solution in appropriate concentration to obtain also 1 wt % of Fe. After water evaporation, the sample was dried at 353 K for 24 h and then calcined in air at 773 K for 3 h.

**2.2. Samples characterization**

Chemical analysis of TEABEA zeolite as well as SiBEA support and Fe-containing samples was done by atomic absorption in Service Central d'Analyse du CNRS, Solaize, France.

The structure of the studied materials was determined by powder X-ray diffraction using BRUKER D8 Advance diffractometer ($CuK_a$ radiation, $\lambda$ = 154.05 pm).

The nature and environment of iron present in FeSiBEA samples were studied by DR UV–vis, Mössbauer and XPS spectroscopies.

DR UV-Vis spectra were recorded at ambient atmosphere on a Cary 5000 Varian spectrometer equipped with a double integrator with polytetrafluoroethylene (PTFE) as a reference.

The local properties of $Fe_{1.0}$SiBEA samples were investigated by means of Mössbauer spectroscopy (MS) employing the $^{57}$Fe gamma resonance transition. A Mössbauer system that consists of the Janis top loaded liquid helium cryostat (Janis Research Company, Wilmington, MA 01887 USA) integrated with a conventional constant-acceleration spectrometer (Science Engineering & Education Co. USA) of the Kankeleit type in transmission geometry was used. During measurements, 100 mCi Mössbauer $^{57}$Co(Rh) γ-ray source and the absorbers were kept at room temperature. The absorbers were made of the fine powdered materials placed in a thin-walled (~0.1 mm) cylindrical plastic containers. The used absorber thicknesses of about 132 mg cm$^{-2}$ were calculated from the optimisation procedure [17]. The resonance 14.4 keV gamma rays (for a given measurement and the energy scale calibration) were detected simultaneously by means of two independent LND Kr/$Co_2$ proportional gas counters attached at opposite sides of the driving system. The drive velocity calibration was performed with a second $^{57}$Co(Rh) source against a standard metallic iron foil at room temperature.

The Mössbauer spectra were analyzed numerically by fitting a hyperfine parameter distribution (HPD) using the Voigt-line-based method of Rancourt and Ping [18]. In this method, the HPD for a given crystal site corresponding to similar structural, chemical and magnetic properties is constructed by a sum of Gaussian components for the quadrupole splitting (QS) distributions and, if necessary, the magnetic hyperfine field $B_{hf}$ distributions. The isomer shift (IS) can be linearly coupled to the primary hyperfine parameters (QS, $B_{hf}$).

The X-ray Photoelectron Spectroscopy (XPS) measurements were carried out with a hemispherical analyzer (SES R4000, Gammadata Scienta, pass energy 100 eV). The unmonochromatized Al$K_\alpha$ X-ray source (1486.6 eV, 11 kV, 17 mA) with no charge neutralizer was applied to generate core excitation. The system was calibrated according to ISO 15472:2001. The energy resolution of the system, measured as a full width at half maximum (FWHM) for Ag $3d_{5/2}$ excitation line, was 0.9 eV. The powder samples were

pressed into indium foil and mounted on a dedicated holder then UHV evacuated. During the measurements, the base pressure in the analysis chamber was about $10^{-9}$ mbar. The area of the sample analysis was approximately 3 $mm^2$. All binding energy (BE) values were charge-corrected to the carbon C 1s excitation set at 285.0 eV. The Shirley-type background subtraction was used to the spectra prior to fitting procedure where Voigt line shape i.e. Gaussian/Lorentzian functional (70:30) was applied. The Fe 2p core excitations were deconvoluted with relative intensity ratio of $2p_{3/2}$ and $2p_{1/2}$ lines fixed to 2:1.

The acidity of SiBEA and $Fe_{1.0}$SiBEA(w) zeolites was investigated by FTIR using CO as a probe molecule. Before CO adsorption experiment, the wafers of SiBEA and $Fe_{1.0}$SiBEA(w) were activated by calcination at 723 K for 2 h in a flow of 2.5 vol. % of $O_2$ diluted in Ar and then outgassed at 573 K ($10^{-3}$ Pa) for 1 h. Following thermal treatment, the samples were cooled down to 100 K. CO was introduced in increasing amounts up to an equilibrium pressure of 133 Pa.

Infrared spectra were recorded using a Bruker Vertex 70 spectrometer (resolution of 2 $cm^{-1}$, 128 scans). The spectra were obtained after subtraction of the spectrum recorded after calcination and prior to CO adsorption.

### 2.3. Catalytic test

Temperature-Programmed Surface Reaction (TPSR) in the temperature range of 298–773 K and linear increase of temperature (5 K $min^{-1}$) was used to measure the catalytic activity. In all experiments the mass of the sample was 0.1 g. The stream of the reacting gases CO/air (0.35 vol. % CO, 99.65 vol. % air) and space velocity 19100 $h^{-1}$ were used.

The concentrations of CO ($CO_2$) or $O_2$ on the outlet of the reactor were measured by the infrared gas analyser (Fuji Electric System Co., type ZRJ-4, detection limit 0.1 ppm) or zirconium oxygen analyser (Z110, Hitech Instruments Ltd Luton England - detection limit 0.1

ppm), respectively. The CO conversion was calculated based on the amount of produced $CO_2$ according to the following equation:

$$\text{CO conversion (\%)} = \frac{C_{CO_2}}{C_{CO}} x100 \quad (1)$$

where: $C_{CO2}$ - concentration of $CO_2$ on the reactor output, $C_{CO}$ - concentration of CO on the reactor input.

### 2.4 TPR - CO measurements

TPR-CO measurements were carried out in PEAK-4 apparatus [19] using CO/He (2 vol. % CO, 98 vol. % He) gas mixture with a flow rate of 50 $cm^3$ $min^{-1}$, in the temperature range of 293-1123 K at a linear temperature ramp of 15 K $min^{-1}$. Prior to the TPR-CO run, the sample of 0.2 g was pre-treated *in situ* by heating in air flow for 1 h at 773 K, followed by cooling to room temperature. The presence of $CO_2$ in the effluent gas was monitored by the $CO_2$ infrared gas analyser (Fuji Electric System Co., type ZRJ-4).

## 3. Results and Discussion

### 3.1. Incorporation of iron into the framework of SiBEA zeolite

#### 3.1.1. X-ray diffraction

Figure 1 shows the XRD patterns of SiBEA, $Fe_{1,0}$SiBEA(w) and $Fe_{1,0}$SiBEA(p) zeolites. All patterns are very similar and no diffraction lines due to other crystalline phases or long-range amorphization of the zeolite are observed. It indicates that the incorporation of iron into the SiBEA matrix does not affect the crystallinity of BEA structure and leads to good dispersion of iron ions. The position change of the narrow main diffraction peak around 2θ of 22.60° is generally taken as evidence of contraction/expansion of the BEA matrix [20, 21]. The decrease of 2θ value from 22.64 (for SiBEA) to 22.58 for $Fe_{1,0}$SiBEA(p) and to 22.56° for $Fe_{1,0}$SiBEA(w) after introduction of iron in the SiBEA indicates expansion of the

BEA matrix and suggests that the iron is incorporated into the framework, in line with our earlier works [22,23]. A little more important expansion of the BEA matrix for $Fe_{1,0}$SiBEA(w) than for $Fe_{1,0}$SiBEA(p) suggests that in the former more amount of iron ions was incorporated in the framework of zeolite than in the latter ones.

### 3.1.2. FTIR studies

The FTIR spectrum of SiBEA in the OH stretching range (Fig. 2) shows three bands at 3739, 3715 and 3530 $cm^{-1}$. The narrow band at 3739 $cm^{-1}$ due to isolated internal silanol groups and broad bands at 3715 $cm^{-1}$ and 3530 $cm^{-1}$ due to terminal internal silanol groups and H-bonded SiOH groups, respectively, reveal the presence of vacant T-atom sites associated with silanol groups in SiBEA, as reported earlier [22, 23].

An incorporation of iron ions into SiBEA involves reduction of the intensity of these bands as shown in Fig. 2**,** suggesting that SiOH groups of vacant T-atoms sites react with Fe ions and leads to the formation of framework pseudo-tetrahedral Fe(III). It is confirmed by appearance of the band at 3630 $cm^{-1}$ (Fig. 2) attributed to ≡Fe(III)-O(H)-Si≡ acidic sites, in line with our earlier work [24].

## 3.2. Nature and environment of iron in FeSiBEA samples

### 3.2.1. DR UV-vis

**Figure 3** shows the DR UV-vis spectra recorded at room temperature of all studied samples $Fe_{1.0}$SiBEA(w), C-$Fe_{1.0}$SiBEA(w), $Fe_{1.0}$SiBEA(p) and C-$Fe_{1.0}$SiBEA(p). In DR UV–vis spectra of as prepared $Fe_{1.0}$SiBEA(w) and $Fe_{1.0}$SiBEA(p) a large band at 272 nm is observed, assigned to the oxygen-to-metal charge transfer transition involving pseudo-tetrahedral Fe(III) as reported earlier [25-29]. Very small broad band at 495 nm can be assigned to mononuclear octahedral Fe(III) species, which is confirmed by disappearing of this band after calcination of $Fe_{1.0}$SiBEA(w) as a result of its dehydration, as shown in Fig. 3

for C-$Fe_{1.0}$SiBEA(w). Moreover, a shift of the band related to pseudo-tetrahedral Fe(III) from 272 to 250 nm indicates the change of the symmetry of the latter, from less distorted to higher distorted pseudo-tetrahedral Fe(III).

In contrast, the behavior of $Fe_{1.0}$SiBEA(p) is different upon calcination. As shown in Fig. 3, besides a similar shift of the band related to pseudo-tetrahedral Fe(III) upon calcination of $Fe_{1.0}$SiBEA(p), there is a small shift of the DR UV-vis band from 495 to 460 nm which is probably related to a slight modification of symmetry of octahedral Fe(III) upon calcination but not disappearing as for C-$Fe_{1.0}$SiBEA(w). It suggests that octahedral Fe(III) present in C-$Fe_{1.0}$SiBEA(p) at 460 nm can be assigned to the presence of extra-framework polynuclear octahedral Fe(III), such as $FeO_x$ oligomers, in line with earlier works [29,30]. Moreover, the pink colour seems to confirm the presence of the latter iron species.

The absence of the band at 460 nm for C-$Fe_{1.0}$SiBEA(w) suggests that all iron in this sample was incorporated into the zeolite framework as pseudo-tetrahedral Fe(III), and as a result sample remained white.

### 3.2.2. $^{57}$Fe Mössbauer spectra (MS)

To obtain more information about white $Fe_{1.0}$SiBEA(w) zeolite sample $^{57}$Fe Mössbauer investigation was performed. The room temperature $^{57}$Fe Mössbauer spectra of $Fe_{1.0}$SiBEA(w) and C-$Fe_{1.0}$SiBEA(w) and their fitted parameters are reported in Fig. 4 and Table 1, respectively. Both samples (containing iron with natural abundance) show pseudo-tetrahedral Fe(III) as main iron species (Fig. 4). The general shape of all spectra is similar. However, their careful analysis reveals some differences concerning the width and asymmetry of the doublets. The spectra are superimposition of at least two Mössbauer signals which can be fitted by symmetric quadrupole doublets using the numerical procedure described above.

The most characteristic feature of doublets showed in Fig. 4 is their low value of isomer shift IS ≤ 0.25 mm $s^{-1}$, which is typical of Fe(III) and strongly suggests tetrahedral surrounding of iron [31-34]. The quadrupole splitting (QS) of iron species are generally in the range of 0.6-1.02 mm $s^{-1}$ with quite reasonable values of the Gaussian width of the QS distribution (σ). The species with lower QS can be attributed to the well-defined framework sites with high symmetry whereas species with higher QS one can rely to the adjacent iron present near to defect sites.

Taking into account the above comments on the $^{57}$Fe Mössbauer spectra (Fig. 4) and the fitted parameters in Table 1, we can assume that in the $Fe_{1.0}$SiBEA(w) two kinds of pseudo-tetrahedral Fe(III) with different symmetry are present. The first kind of pseudo-tetrahedral Fe(III) labelled as ($Fe_{Td1}$) for which the value of QS is 0.64 mm $s^{-1}$, are relatively less distorted pseudo-tetrahedral Fe(III). In contrast, the second kind of pseudo-tetrahedral Fe(III) labelled as ($Fe_{Td2}$) for which the value of QS is 1.01 mm $s^{-1}$ may be attributed to more distorted pseudo-tetrahedral Fe(III).

The formation of two kinds of pseudo-tetrahedral Fe(III) species seems to correlate with the presence of two kinds of framework Al($T_d$) sites present in the initial BEA zeolite, identified by $^{27}$Al MAS NMR in our previous work [35]. As reported in [35-39], two kinds of tetrahedral Al sites corresponding to two specific T-positions occurred in BEA structure, containing nine different types of T sites (T1-T9). The part of these sites can be more readily substituted by iron atoms in the BEA framework then others. In the paper quoted above [35] we have showed that T1 and T2 sites are relatively stable and resistant to dealumination by nitric acid.

After incorporation of Fe ions into the SiBEA framework and then calcination of as prepared Fe-containing SiBEA zeolite, the geometrical parameters of T sites can change. The DR UV-vis results presented above show that one can distinguish only two kinds of T sites

occupied by iron: less distorted pseudo-tetrahedral Fe(III) and more distorted pseudo-tetrahedral Fe(III), which is in line with Mössbauer results.

The length of Fe-O bonds and the values of O-Fe-O angles in the basic building units ($FeO_4$) in strongly distorted pseudo-tetrahedral Fe(III) differ significantly from that in well-defined, less distorted pseudo-tetrahedral Fe(III). It suggests that strongly distorted pseudo-tetrahedral Fe(III) are less stable and could easier change its coordination and therefore posses better catalytic properties than less distorted pseudo-tetrahedral Fe(III).

The analysis of the results presented in Table 1 shows that in $Fe_{1.0}$SiBEA(w), the majority (61 %) of iron in the zeolite framework is present as less distorted pseudo-tetrahedral Fe(III) ($Fe_{Td1}$) sites whereas only 39 % as strongly distorted pseudo-tetrahedral Fe(III) ($Fe_{Td2}$) sites.

The most remarkable difference between calcined and non–calcined $Fe_{1.0}$SiBEA(w) samples is the proportion of ($Fe_{Td1}$) to ($Fe_{Td2}$) sites. After calcination the C-$Fe_{1.0}$SiBEA(w) sample contains only about 32 % of ($Fe_{Td1}$) sites whereas the rest is present as ($Fe_{Td2}$). Such results suggest that some part of ($Fe_{Td1}$) is transformed into ($Fe_{Td2}$) sites during the calcination process. Thus, $^{57}$Fe Mössbauer spectroscopy allowed to distinguish between two kinds of pseudo-tetrahedral Fe(III) species with various degrees of distortion upon calcination process. It can be understood if we consider that calcination in air at 773 K can strongly affect the symmetry of pseudo-tetrahedral Fe(III) in framework of Fe-containing BEA zeolites formed by reaction of iron precursor with silanol groups of vacant T-atom sites.

The results presented above are in line with earlier work [24], where we have evidenced by DR UV-vis, Mössbauer and XAS spectroscopies the presence of only framework pseudo-tetrahedral Fe(III) species in $Fe_x$SiBEA zeolites with lower than 2 wt % of Fe. Moreover, the latter technique has allowed to distinguish in Fourier transforms (not phase shift-corrected) of $Fe_{0.5}$SiBEA, $Fe_{1.0}$SiBEA and $Fe_{2.0}$SiBEA zeolites two peaks at about 1.5-

1.7 Å assigned to two contributions of the Fe-O shell. It has been suggested that in those zeolites there were two kinds of pseudo-tetrahedral Fe(III) sites with different symmetry like in $Fe_{1.0}$SiBEA(w) obtained in this work.

### 3.2.3. XPS results

The high resolution spectra of Fe 2p, Si 2p, O 1s and C 1s core excitations were acquired for $Fe_{1.0}$SiBEA(w) and C-$Fe_{1.0}$SiBEA(w).

The Si 2p spectra of $Fe_{1.0}$SiBEA(w) and C-$Fe_{1.0}$SiBEA(w) are shown in Fig. 5. The Si 2p core levels are splitted into $2p_{3/2}$ and $2p_{1/2}$ components due to the spin—orbit coupling. The Si 2p BE values (103.9 – 104.1 eV) close to that reported earlier for BEA, MFI and MOR zeolites are related to the presence of tetrahedral Si(IV) [40-46]. The O 1s lines can be decomposed into three components: a main peak close to 533.2 – 533.3 eV (assigned to oxygen in the zeolite framework and adsorbed water), a much smaller peak at 530.7–531.0 eV due to oxygen–metal bonds and a peak at 534.1–534.3 eV (Fig.6) assigned to oxygen in organic contaminants. The C 1s core lines are composed of four peaks at 285.0 eV (C-C structural bonds in organic contaminants), 286.2 eV (C-O groups), 287.8–288.3 eV (C=O groups) and 289.8–290.2 eV (carboxyl group and carbonates).

The Fe 2p spectra of $Fe_{1.0}$SiBEA(w) and C-$Fe_{1.0}$SiBEA(w) are shown in Fig. 7. The iron 2p core levels are split into $2p_{3/2}$ and $2p_{1/2}$ doublets due to the spin-orbit coupling. It has been shown in literature that Fe $2p_{3/2}$ and Fe $2p_{1/2}$ binding energies and the value of doublet splitting are strongly dependent on the iron ionic states [47-51]. One should bear in mind that both Fe(III) and Fe(II) species in oxide lattice can show so called shake-up satellites, although sometimes they are not present as were reported for $Fe_3O_4$ [52]. Moreover, the positions of shake-up satellites are also sensitive to the oxidation state of iron. All these features can be used for qualitative analysis of the Fe oxidation states in studied zeolite materials.

To describe spectra of $Fe_{1.0}$SiBEA(w) and C-$Fe_{1.0}$SiBEA(w) properly, it was necessary to use satellites for each single component of Fe $2p_{3/2}$ and Fe $2p_{1/2}$ lines. The satellites are rather clearly distinguishable, unfortunately they overlap energetically the main photoelectron Fe 2p excitations. Moreover, the photoelectron peaks are significantly broadened and show asymmetric high-BE side. Taking into account all above mentioned comments, both analyzed Fe 2p spectra were fitted by a single photoelectron doublet and its associated satellites (Fig. 7 and Table 2). One can find that the binding energies of the Fe 2p peaks and its satellites in both samples are very similar. The spin-orbit splittings of doublets are in the range of 13.0-13.2 eV, which was observed in several iron oxides and zeolites recently [53-58].

It is well known that BE of Fe $2p_{3/2}$ higher than 710.2 eV can be assigned to Fe(III) species. Thus, one can conclude that all components should be assigned to ferric species. Taking into account qualitative comparison of results obtained by $^{57}$Fe Mössbauer spectroscopy and XPS one can identify main components of the spectra to the Fe(III) species in pseudo-tetrahedral surroundings. Unfortunately, rather poor signal to noise ratio (due to a very low content of iron) does not distinguish between ($Fe_{Td1}$) and ($Fe_{Td2}$) sites. However, the significant broadening of Fe 2p core excitation lines strongly suggest that there might be two states in the samples, one being Fe(III) not included in the framework (UV-Vis at 495 eV), with lower BE and the other one being an intra-framework Fe. The slight shift of the signal to higher BE after calcination might support this idea. It is worth mentioning, that some features seen in Mössbauer spectra (Fig. 4) i.e. decreasing of isomer shift, can probably be related to the appropriate differences in the spin-orbit splittings and BE shift of satellites.

### 3.3. Acidity of FeSiBEA zeolites

The acidity of C-$Fe_{1.0}$SiBEA(w) was investigated by FTIR using CO as probe molecule. Introduction of CO (100 Pa equilibrium pressure) into C-$Fe_{1.0}$SiBEA(w) at 100 K

leads to shift of the original hydroxyl bands into lower wavenumbers and to appearance of the bands at 3640, 3443 and 3284 $cm^{-1}$ (Fig. 8, spectrum a). The intensity of the band at 3640 $cm^{-1}$ quickly decreases with the CO pressure and the band at 3739 $cm^{-1}$ is restored. The observed shift of this band of 99 $cm^{-1}$ indicates a weak acidity of the 3739 $cm^{-1}$ internal isolated silanol groups present in C-$Fe_{1.0}$SiBEA(w). A shoulder observed at 3590 $cm^{-1}$ ( Fig. 8, spectra b-d), related probably to the 3715 $cm^{-1}$ isolated silanol groups, disappered very fastly upon outgassing of C-$Fe_{1.0}$SiBEA(w). However, the corresponding CO complex is more stable than that giving the band at 3640 $cm^{-1}$. Thus, we conclude that some internal isolated silanols have an enhanced acidity. The appearance of two shifted bands at 3443 and 3284 $cm^{-1}$ indicates some heterogeneity of the Brønsted acidic sites. It seems that the former band is related to hydrogen bonded silanols observed in original IR spectrum of $Fe_{1.0}$SiBEA(w) at 3530 $cm^{-1}$ (Fig. 2) characterised by weak Brønsted acidity ($\Delta\nu$ = 87 $cm^{-1}$) and the latter is related to much stronger Brønsted acidity related to ≡Fe(III)-O(H)-Si≡ acidic sites observed in original IR spectrum of $Fe_{1.0}$SiBEA(w) at 3630 $cm^{-1}$ (Fig. 2) ($\Delta\nu$ = 346 $cm^{-1}$).

Fig. 9 shows the changes in the carbonyl range when CO is adsorbed on C-$Fe_{1.0}$SiBEA(w). Under CO equilibrium pressure of 100 Pa, seven carbonyl bands are detected at 2220, 2190, 2175, 2157, 2140, 2135 and 2095 $cm^{-1}$ (Fig. 9, spectrum a). The bands at 2140 and 2135 $cm^{-1}$ are assigned to weakly bonded, physically adsorbed CO, which disappear firstly upon outgassing (Fig. 9, spectra b and c). The next band which disappears is that at 2157 $cm^{-1}$. Its intensity correlates with that of the band appeared at 3640 $cm^{-1}$ (Fig. 8) allowing assigning the band at 2157 $cm^{-1}$ IR band to CO bonded to internal isolated silanol groups. Further outgassing of C-$Fe_{1.0}$SiBEA(w) provokes disappearance of the carbonyl band at 2175 $cm^{-1}$ (Fig. 9, spectra c-e) which could be assigned to CO polarized by the acidic ≡Fe(III)-O(H)-Si≡ groups. The wavenumber of this band is typical of CO interacting with bridging zeolite hydroxyls. Two bands of low intensity at 2190 and 2220 $cm^{-1}$ do not

correlate with any OH band and thus, are assigned to iron carbonyls. The band at 2220 $cm^{-1}$ could be assigned to Fe(III)-CO species, in line with our earlier work [56]. In contrast, the band at 2190 $cm^{-1}$ could be related to CO adsorbed on isolated framework Fe(II) formed from Fe(III) upon interaction with CO, in agreement with our earlier suggestion [56].

### 3.4. Catalytic activity

Figure 10 shows the temperature-dependence of CO conversion in CO oxidation by air on C-$Fe_{1.0}$SiBEA(w), C-$Fe_{1.0}$SiBEA(p) and 1%Fe/$SiO_2$ catalysts. The profiles depict a typical light–off character of the temperature-programmed surface reaction. The results presented in Fig. 10 prove that the catalytic activity of all investigated samples is rather low and changes in the row:

$$Fe_{1.0}SiBEA(w) > Fe_{1.0}SiBEA(p) > 1\%Fe/SiO_2$$

Such results confirm earlier findings that catalytic activity in CO oxidation strongly depends on the state of iron present in the investigated catalysts [14]. Taking into consideration results described above we can assume that in the C-$Fe_{1.0}$SiBEA(w) strongly distorted pseudo-tetrahedral Fe(III) predominate. As shown by DR UV-vis (Fig. 2) C-$Fe_{1.0}$SiBEA(p) contains of framework pseudo-tetrahedral Fe(III), extra-framework octahedral Fe(III) and $FeO_x$ oligomers, while the 1%Fe/$SiO_2$ contains only $FeO_x$ oligomers and/or $Fe_yO_x$ oxides (result not shown).

Thus, the higher catalytic activity of C-$Fe_{1.0}$SiBEA(w) than C-$Fe_{1.0}$SiBEA(p) in CO oxidation may be related to the presence in the former mainly strongly distorted framework pseudo-tetrahedral Fe(III) (Fig. 3). In contrast, the presence in C-$Fe_{1.0}$SiBEA(p) of other forms of Fe(III) species, such as extra-framework octahedral Fe(III) and/or Fe oligomers (Fig. 3) is a reason of its lower activity than C-$Fe_{1.0}$SiBEA(w). Thus, the presence of such kinds of Fe(III) species leads to lower conversion of carbon monoxide. From this point of view it is

obvious that 1%Fe/$SiO_2$ sample, which contains almost only iron oxides shows the lowest catalytic activity.

The concentration of extra-framework octahedral Fe(III) and $FeO_x$ oligomers increases with the increasing of iron loading in $Fe_x$SiBEA what in turn leads to the decrease of catalytic activity. It was shown in our previous paper [14], where a gradual decrease in the catalytic activity with an increase of iron content (in the range of 1 -10 wt %) was observed.

As it was mentioned above, the catalytic activity of all investigated samples is rather low. It is probably associated with the lack of sufficiently strong adsorption sites for CO and/or $O_2$ molecules. In order to describe the mechanism of catalytic CO oxidation it is necessary to point out the adsorption sites for CO and/or $O_2$ molecules. Coordinatively saturated Fe(III) species are not able to interact with probe molecules in contrast to Fe(II) species which can adsorb both oxygen and carbon monoxide [15, 16].

The Mössbauer spectrum of the most catalytic active C-$Fe_{1.0}$SiBEA(w) shows no traces of Fe(II) species (Fig. 4). Hence, it can be assumed that also $Fe_{1.0}$SiBEA(p) and 1%Fe/$SiO_2$ samples do not contain a detectable amount of Fe(II) species. This explains why the catalytic activity of the investigated samples is low, but does not explain why the $Fe_{1.0}$SiBEA(w) sample in which Fe(III) species in pseudo-tetrahedral coordination predominate, is more active than the others.

As it was shown earlier (Section 3.2.2) calcination of $Fe_{1.0}$SiBEA(w) in air at 773 K strongly affects the symmetry of pseudo-tetrahedral Fe(III) in the framework of Fe-containing BEA zeolites. After this process the concentration of Fe(III) present in C-$Fe_{1.0}$SiBEA(w) as less distorted pseudo-tetrahedral Fe(III) ($Fe_{Td1}$) is only half of that present in $Fe_{1.0}$SiBEA(w).

Thus, it can be assumed that the most active centres in CO oxidation over $Fe_{1.0}$SiBEA catalyst are strongly distorted isolated pseudo-tetrahedral Fe(III). In our opinion these centres should show a special structure, which ensures that the Fe(III) species are i) easily available

for interaction with CO, ii) easily reducible, iii) easily oxidized and iv) remain stable in the reduction –oxidation cycle.

Considering these statements we propose a model of the active centre structure in C-$Fe_{1.0}$SiBEA(w) catalyst. This structure is related to the structure of the Al($T_d$) sites present in the initial BEA zeolites.

The unit cell of zeolite BEA (the periodic building unit (PBU)) consists of nine structurally different T atom sites with tetrahedral coordination. These sites are placed in PBU of BEA zeolite in the manner shown in Fig.11, and are usually classified into three groups: i/ T1 and T2 sites associated with one of four-membered rings (4MR), ii/ T3 -T6 sites associated with two of 4MR and iii/ T7- T9 sites situated in fused 5- and 6-rings [59-63].

In the Section 3.2.2 basing on [35-39] works, it was claimed that the T1 and T2 sites are more stable and resistant to dealumination by nitric acid than T3-T9 ones. Therefore, it was stated that distribution of aluminum atoms in the BEA framework is non-random and two main types of aluminum tetrahedral sites are present. The authors of the quoted works assume that stability of T1 and T2 sites results from the fact that they are situated in four-membered rings, which exhibit the largest strain with the biggest T-O-T angle [62]. In addition, van Bokhoven et al. [62] have shown by $^{27}$Al MQ MAS NMR that aluminium atoms present in T1 and T2 sites are not able to adopt an octahedral coordination and are resisted to dealumination even during steaming at 500 °C. Thus, two kinds of tetrahedral Al sites present in the BEA zeolite have been distinguished and basing on van Bokhoven [62] and our previous work [35] we can conclude that T1 and T2 sites are more stable than other ones. One can expect that after dealumination of the BEA zeolite, iron incorporated into vacant T1-T9 sites will show the similar properties as aluminium in these sites.

The results of Mössbauer measurements shown in Section 3.2.2 proved that in the $Fe_{1.0}$SiBEA(w) two kinds of pseudo-tetrahedral Fe(III) with different symmetry are present.

Therefore the tetrahedral Fe(III) present in the T1 and T2 positions should be less prone to distortion and present in the FeSiBEA zeolite as less distorted pseudo-tetrahedral Fe(III) labelled earlier as $Fe_{Td1}$. These sites are coordinatively saturated and catalytically non-active. Figure 12 shows the structure of $Fe_{Td1}$ present in four-membered rings (4MR) located in the T1 or T2 position. The geometry of this structure favours the stability of $Fe_{Td1}$ even though iron in this site is stressed. Its stability is connected with the stability of acidic bridging hydroxyls groups ≡Fe(III)-O(H)-Si≡, which are characterized by the IR band at 3630 $cm^{-1}$ (**Section** 3.1.2). These hydroxyl groups are the part of ($Fe_{Td1}$) sites.

It should be noted that the elimination of these groups could caused total, non-reversible distortion of $Fe_{Td1}$ sites. Thus, these bridging hydroxyls groups should be very stable and both the process of calcination or reduction carried out at moderately high temperatures should not removed them. This conclusion is in line with our earlier results presented in work [15]. The results presented there proved that the reduction of the FeSiBEA samples hardly affects their coverage with hydroxyl groups. Nevertheless, IR band at 3630 $cm^{-1}$ remains practically unaffected up to the temperature of reduction of 673 K. Thus, one can assume that these bridging hydroxyls groups are very stable and neither the process of calcination nor reduction carried out at moderately high temperature do not eliminate them. Thus, the presence of bridging hydroxyls groups in the FeSiBEA samples after their heating treatment also in reduction gas atmosphere can be prove of the presence of $Fe_{Td1}$ sites, their high stability and coordinatively saturated character. Taking into account these statements it is clear that the iron ions incorporated into the T1 and T2 sites cannot be precursors of active centres in CO oxidation over $Fe_{1.0}$ SiBEA(w) catalyst.

It seems that the most probable active centres of CO oxidation are pseudo-tetrahedral Fe(III) in T8 position, which are included into the six-membered rings simultaneously being external sites in 12 - membered rings (Fig. 13 (a)). We believe that from the geometric reason

pseudo-tetrahedral Fe(III) site in T8 position is more prone to the reversible distortion than this site present in other positions. Taking into account the above discussion we propose the model of the active centre located in T8 position.

Figure 13 (a) shows the structure of the precursor of the active centre - less distorted pseudo-tetrahedral Fe(III) site ($Fe_{Td1}$) included into six-membered rings and located in the T8 position. Such $Fe_{Td1}$ sites become catalytically active after calcination, which therefore can be considered as the process of $Fe_{1.0}$SiBEA(w) catalyst activation. Figure 13 (b) shows how this structure transforms during the calcination. As a result of this process, strongly distorted pseudo-tetrahedral Fe(III) sites ($Fe_{Td2}$) are formed. We suggest that these sites are active centres in the process of CO oxidation over $Fe_{1.0}$SiBEA(w) zeolite. The calcination could lead to dehydroxylation of $Fe_{1.0}$SiBEA(w) sample. Bridging hydroxyl groups ≡Fe(III)-O(H)-Si≡, present between T8 and T6 sites could be in this case eliminated. In the result, less distorted pseudo-tetrahedral Fe(III) ($Fe_{Td1}$site) located in the T8 position could be transformed into strongly distorted pseudo-tetrahedral Fe(III) ($Fe_{Td2}$site) and concentration of the latter sites could be increased. These suggestions are in line with the results obtained by Mössbauer spectroscopy for as prepared and calcined $Fe_{1.0}$SiBEA(w) presented in Table 2 (see Section 3.2.2.).

To summarize, one can conclude, the total inactivity of the tetrahedral Fe(III) due to their coordinative saturation [15,16] is true only for ($Fe_{Td1}$) sites which are located mainly in T1 and T2 positions. However, pseudo--tetrahedral Fe(III), located in T8 positions due to their strong distortion can be catalytic active sites. Although the pseudo-tetrahedral character remains (Fig. 13 (b)), Fe-O bonds are weakened, thermodynamically unstable and in the presence of reductive gas molecules, like CO, pseudo-tetrahedral Fe(III) ($Fe_{T2}$ sites) can interact with them creating Fe(III)-CO species. In this aspect, the results of FeSiBEA acidity presented in Section 3.3 seem to be very interesting. As it was discussed earlier, two bands

of low intensity at 2220 and 2190 $cm^{-1}$ not correlating with any OH band and assigned to iron carbonyls can be observed. These iron carbonyls arise as a result of the interaction between strongly distorted pseudo-tetrahedral Fe(III) and CO. Thus, the IR band at 2220 $cm^{-1}$ appeared at Fig. 8 after adsorption of CO on C-$Fe_{1.0}$SiBEA(w) could be assigned to Fe(III)-CO species. The band at 2190 $cm^{-1}$ was related to CO adsorbed on isolated framework Fe(II) formed from Fe(III) upon interaction with CO. Thus, these IR measurements confirm that strongly distorted pseudo-tetrahedral Fe(III) can interact with CO with creating Fe(III)-CO species which could be transformated into strongly distorted pseudo-tetrahedral Fe(II) as a result of reduction with CO.

On the other hand, one can expect that the creation of strongly distorted pseudo-tetrahedral Fe(II) will be easier for more reducible samples. TPR-CO profiles of C-$Fe_{1.0}$SiBEA(w), C-$Fe_{1.0}$SiBEA(p) and for comparison 1%Fe/$SiO_2$ samples are presented on Fig. 14. For C-$Fe_{1.0}$SiBEA(w) catalyst the reduction starts at lower temperature and the amount of CO consumed is significantly higher than in the case of C-$Fe_{1.0}$SiBEA(p). TPR-CO profile of a 1%Fe/$SiO_2$ catalyst shows that iron oxide in this sample is hardly reducible, its reduction starts only at about 800 K and the amount of $CO_2$ emitted, as the product of reduction, is very low. Iron oxide supported on $SiO_2$ is more difficult to reduction than iron in the framework of SiBEA zeolite. In the case of 1%Fe/$SiO_2$ catalyst, the low concentration of supported iron favours FeO and Fe-Si compounds formation. Moreover, during iron oxides reduction by carbon monoxide the formation of iron carbide may occur as the results of Fe - CO interaction (adsorption and dissociation of CO). The metallic iron converts to iron carbide already at the temperature about 573 K, so it is possible that the process of iron oxides reduction can be stopped as a result of iron carbide phase formation. This mechanism is very well proved as a part of Fischer-Tropsch synthesis carried out on iron catalysts [64-66]. It is why carbon monoxide is not a good reducing gas for iron catalyst. Nevertheless, we used CO

in order to avoid the introduction of hydroxyl groups to the zeolite structure which could take place if hydrogen was used as a reducing agent.

Such results prove that $Fe_{1.0}$SiBEA catalyst contains iron mainly in the form of isolated homogeneously distributed pseudo-tetrahedral Fe(III) present as framework T-atom sites. If it were not a case, the reduction of $Fe_{1.0}$SiBEA would also be difficult like that of $Fe/SiO_2$ since the formation of iron carbide phase occurs on iron clusters but not isolated atoms. Figure 13 (c) shows the state of $Fe_{Td2}$ sites after reduction which appears as strongly distorted pseudo-tetrahedral Fe(II). It seems that pseudo-tetrahedral character of $Fe_{Td2}$ sites remains after their reduction.

Based on the discussion presented above, it seems that process of Fe(III) reduction in $Fe_{1.0}$SiBEA samples conducted at elevated temperatures will mainly concern strongly distorted pseudo-tetrahedral Fe(III). As a result, both the creation of Fe(II) in pseudo-tetrahedral coordination and the increase in the catalytic activity are expected.

To obtain the diversified concentration of pseudo-tetrahedral Fe(II) sites, both C-$Fe_{1.0}$SiBEA and $1\%Fe/SiO_2$ catalysts were subjected to the reduction in CO at different temperatures (473, 573, 673 and 773 K) for 15 min. Figure 15 shows the conversion of CO as a function of temperature for $Fe_{1.0}$SiBEA(w) sample reduced in 2 vol. % CO, 98 vol. % He gas mixture at different temperatures. The process of CO oxidation consists of two distinct stages and the conversion in the first stage clearly increases with rising of the reduction temperature. In the first one, the process of CO oxidation starts at ca. 363 K and distinct conversion maximum at about 413 K is observed. The second stage starts at about 523 K and it is the same temperature which was recorded for $Fe_{1.0}$SiBEA(w) catalyst (Fig. 10). Similar experiment performed for $Fe_{1.0}$SiBEA(p) and $1\%Fe/SiO_2$ catalysts showed only one-stage process. The obtained profiles of TPSR unequivocally suggest that the reduction of C-$Fe_{1.0}$SiBEA(w) catalyst leads to the creation of new catalytic sites. These sites are created as a

result of the reduction of strongly distorted pseudo-tetrahedral Fe(III) into pseudo-tetrahedral Fe(II). The above results show that catalytic activity of the reduced Fe1.0SiBEA(w) strongly depends on the presence and concentration of pseudo-tetrahedral Fe(II). These pseudo-tetrahedral Fe(II) seem to be active sites of CO oxidation on the C-$Fe_{1.0}$SiBEA(w) catalyst. They arise as prodact interaction of CO with strongly distorted pseudo-tetrahedral Fe(III) ($Fe_{Td2}$). These strongly distorted pseudo-tetrahedral Fe(III) show higher ability to be reduced to the active sites in the reaction with CO than the other iron species in FeSiBEA zeolites or in Fe/$SiO_2$ catalyst.

**4. Conclusions**

The precursors of the active centres of CO oxidation over $Fe_{1.0}$SiBEA(w) catalyst are strongly distorted pseudo-tetrahedral Fe(III) ($Fe_{Td2}$) sites well dispersed in the framework of SiBEA zeolite.

These strongly distorted pseudo-tetrahedral Fe(III) ($Fe_{Td2}$) sites can interact with CO and, as a result, pseudo-tetrahedral Fe(II) are formed which are the active sites of CO oxidation on $Fe_{1.0}$SiBEA(w) catalyst.

Less distorted pseudo-tetrahedral Fe(III) ($Fe_{Td1}$) sites present in $Fe_{1.0}$SiBEA(w) catalyst and other kinds of iron species present in FeSiBEA(p) and 1%Fe/$SiO_2$ catalysts are much strongly resisted to reduction and by this reason are less active in CO oxidation.

Further studies over FeSiBEA catalysts are undertaken to evidence the formation of such pseudo-tetrahedral Fe(II) sites extremely active in CO oxidation at lower temperatures and to show their unusual properties in CO oxidation. The studies are in progress and the results will be described in our next paper.

**Acknowledgement**

The research was carried out with the Mössbauer equipment purchased thanks to the financial support of the European Regional Development Fund in the framework of the Polish Innovation Economy Operational Program (contract no. POIG.02.01.00-12-023/08).

**Refernces**

[1] G. Dong, J. Wang, Y. Gao, S. Chen, Catal. Letters 58 (1999) 37-41.

[2] N. D Gangel, N. M. Gupta, R. M. Iyer, J. Catal. 126 (1990) 13-25.

[3] J. Ch. Crump, J.D. Gilbertson, B.D. Chandler, Topic. Catal. 49 (2008) 233-240.

[4] I. Dobrosz-Gomez, I. Kocemba, J. Rynkowski, Appl. Catal. B 83 (2008) 240-255.

[5] Rui Lin, Meng-Fei Luoa, Yi-Jun Zhonga, Zong-Lan Yan, Guang-Yu Liu, Wei-Ping Liu, Appl. Catal. A 255 (2003) 331-336.

[6] X. Liu et al. Catal. Comm. 12 (2011) 530–534.

[7] L.D. Li, Q. Shen, J.J. Yu, Z.P. Hao, Z.P. Xu, G.Q. Max Lu, Environ. Sci. Technol. 41 (2007) 7901-7906.

[8] L. Gutierrez, M.A. Ulla, E.A. Lombardo, A. Kovacs, F. Lonyi, J. Valyon, Appl. Catal. 292 (2005) 154-161.

[9] L. Capek, J. Dedecek, B. Wichterlova, J. Catal. 227 (2004) 352-366.

[10] S. Dzwigaj, J. Janas, T. Machej, M. Che, Catal. Today 119 (2007) 133-136.

[11] G. Yang, J. Guan, L. Zhou, X. Han, X. Bao, Catal. Surv. Asia, 14 (2010) 85-94.

[12] A.Mette Frey, S. Mert, J. Due-Hansen, R. Fehrmann, C. Christensen, Catal. Lett. 130 (2009) 1-8.

[13] S. Malykhin, V. F. Anufrienko, J. Hansen, V. Kuznetsova, V. Larina, G. M. Zhidomirov, J. Struct. Chem. 48 (2007) 855-861

[14] I. Hnat, I. Kocemba, J. Rynkowski, T. Onfroy, S. Dzwigaj, Catal. Today, 176 (2011) 229-233.

[15] K. Hadjiivanov, E. Ivanova, R. Kefirov, J. Janas, A. Plesniar, S. Dzwigaj, M. Che, Micropor. Mesopor. Mater. 131 (2010) 1-12.

[16] A. Zecchina, F. Geobaldo, C. Lamberti, S. Bordiga, G. Turnes Palomino, C. Otero Arean, Catal. Lett. 42 (1996) 25-33.

[17] G. J. Long, T. E. Cranshaw, G. Longworth, Mössbauer Effect Reference and Data Journal 6 (1983) 42-49.

[18] D.G. Rancourt, J.Y. Ping, Nucl. Instrum. Meth. Phys. Rev. B 58 (1991) 85-97.

[19] I. Kocemba, Przemysł Chemiczny 82 (2003) 142-145.

[20] M.A. Camblor, A. Corma, J. Pérez-Pariente, Zeolites 13 (1993) 82-87.

[21] J.S. Reddy, A. Sayari, Stud. Surf. Sci. Catal. 94 (1995) 309-316.

[22] S. Dzwigaj, M.J. Peltre, P. Massiani, A. Davidson, M. Che, T. Sen, S. Sivasanker, Chem. Commun. (1998) 87-88.

[23] S. Dzwigaj, P. Massiani, A. Davidson, M. Che, J. Mol. Catal. 155 (2000) 169-182.

[24] S. Dzwigaj, J. Janas, J. Gurgul, R.P. Socha, T. Shishido, M. Che, Applied Catalysis B 85 (2009) 131-138.

[25] L. Capek, V. Kreibich, J. Dedecek, T. Grygar, B. Wichterlova, Z. Sobalik, J.A. Martens, R. Brosius, V. Tokarova, Micropor. Mesopor. Mater. 80 (2005) 279-289.

[26] J. Perez-Ramirez, J.C. Groen, A. Brückner, M.S. Kumar, U. Bentrup, M.N. Debbagh, L.A. Villaescusa, J. Catal. 232 (2005) 318-334.

[27] M. Schwidder, S. Heikens, A. De Toni, S. Geisler, M. Berndt, A. Brückner, W. Grünert, J. Catal. 259 (2008) 96-103.

[28] P. Balle, B. Geiger, S. Kureti, Appl. Catal. B 85 (2008) 109-119.

[29] M.S. Kumar, M. Schwidder, W. Grünert, U. Bentrup, A. Brückner, J. Catal. 239 (2006) 173-186.

[30] M.S. Kumar, M. Schwidder, W. Grünert, U. Bentrup, A. Brückner, J. Catal. 223 (2004) 384-397.

[31] R.G. Burns, Hyperfine Interactions 91 (1994) 739-745.

[32] R.M. Mihályi, K. Lázár, M. Kollár, F. Lónyi, G. Pál-Borbély, Á. Szegedi, Micropor. Mesopor. Mater. 110 (2008) 51-63.

[33] P. Fejes, J.B. Nagy, K. Lázár, J. Halász, Appl. Catal. A 190 (2000) 117-135.

[34] P. Fejes, I. Kiricsi, K. Lázár, I. Marsi, A. Rockenbauer, L. Korecz, Appl. Catal. A 242 (2003) 63-76.

[35] R. Hajjar, Y. Millot, P. Man, M. Che, S. Dzwigaj, J. Phys. Chem. C 112 (2008) 20167-20175.

[36] L.C. de Menorval, L. W. Buckermann, F. Figueras, F. Fajula, J. Phys. Chem. 100 (1996) 465-467

[37] G. Valerio, A. Goursot, R. Vetrivel, O. Malkina, V. Malkina, D.R. Salahub, J. Am. Chem. Soc. 120 (1998) 11426 –11431

[38] N.Y. Chen, W.E. Garwood, F.G. Dwyer, Shape Selective Catalysis in Industrial Applications, second ed., Dekker, New York, 1996.

[39] M.W. Deem, J.M. Newsam, J.A. Creighton, J. Am. Chem. Soc. 114 (1992) 7198-7207.

[40] K. Arishtirova, P. Kovacheva, A. Predoeva, Appl. Catal. A 243 (2003) 191-196.

[41] P. Kovacheva, K. Arishtirova, A. Predoeva, React. Kinet. Catal. Lett. 79 (2003) 149-155.

[42] L.P. Oleksenko, Theor. Exp. Chem. 40 (2004) 331-336.

[43] L. Meda1, G. Ranghino, G. Moretti,G. F. Cerofolini, Surf. Interface Anal. 33 ( 2002) 516–521.

[44] W. Grünert, R. Schlögl, Mol. Sieves 4 (2004) 467-515.

[45] J. Janas, T. Machej, J. Gurgul, R.P. Socha, M. Che, S. Dźwigaj, Appl. Catal. B 75 (2007) 239-248.

[46] P. Boroń, L. Chmielarz, J. Gurgul, K. Łątka, T. Shishido, J.-M. Krafft, S. Dzwigaj, Appl. Catal. B 138–139 (2013) 434 -445.

[47] M. Descostes, F. Mercier, N. Thromat, C. Beaucaire, M. Gautier-Soyer, Appl. Surf. Sci. 165 (2000) 288-302.

[48] T.-C. Lin, G. Seshadri, J.A. Kelber, Appl. Surf. Sci. 119 (1997) 83-92.

[49] T. Yamashita, P. Hayes, Appl. Surf. Sci. 254 (2008) 2441-2449.

[50] P.C.J. Graat, M.A.J. Somers, Appl. Surf. Sci. 100/101 (1996) 36-40.

[51] Th. Schedel-Niedrig, W. Weiss, R. Schlögl, Phys. Rev. B 52 (1995) 17449-17460.

[52] [ M. Muhler, R. Schlögl, G. Ertl, J. Catal. 138 (1992) 413-444.

[53] P. Fejes, I. Kiricsi, K. Kovács, K. Lázár, I. Marsi, A. Oszkó, A. Rockenbauer, Z. Schay, Appl. Catal. A 223 (2002) 147.

[54] J. Janas, J. Gurgul, R.P. Socha, T. Shishido, M. Che, S. Dzwigaj, Appl. Catal. B 91 (2009) 113-122.

[55] R.B. Borade, A. Clearfield, Micropor. Mater. 2 (1994) 167-177.

[56] P. Boron, L. Chmielarz, J. Gurgul, K. Latka, B. Gil, J.M. Krafft, S. Dzwigaj, Catal. Today 235 (2014) 210-225.

[57] J. Gurgul, K. Łątka, I. Hnat, J. Rynkowski, S. Dzwigaj, Micropor. Mesopor. Mater. 168 (2013) 1-6.

[58] P. Boroń, L. Chmielarz, J. Gurgul, K. Łątka, B. Gil, B. Marszałek, S. Dzwigaj, Micropor. Mesopor. Mater. 203 (2015) 73-85.

[59] I. Papai, A. Goursot, F. Fajula, J. Weber, J. Phys. Chem. 98 (1994) 4654-4659.

[60] International Zeolite Association, Structure Commission, http://www.iza-structure.org.

[61] J. A. van Bokhoven, D.C. Koningsberger, P. Kunkeler, H. van Bekkum, A.P.M. Kentgens, J. Am. Chem. Soc. 122 (2000) 12842-12847.

[62] C. Baerlocher W. Meier, D.H. Olson, Atlas of Zeolite Framework Types, Elsevier Amsterdam, 2007, p. 72.

[63] T. I. Koranyi, J. B. Nagy, J. Phys. Chem. B 110 (2006) 14728-14735.

[64] M. D. Shroff, D. S. Kalakkad, A. G. Sault, A. K. Datye, J. Catal., 156 (1995) 185-207.

[65] R. A. Dictor, A. T. Bell, J. Catal., 97 (1986) 121-136.

[66] A. Loaiza-Gil, B. Fontal, F. Rueda, Appl. Catal. A, 177 (1999) 193-203.

**Table 1**. Hyperfine parameters derived from the room-temperature Mössbauer spectra for $Fe_{1.0}$SiBEA(w) and C-$Fe_{1.0}$SiBEA(w) samples. Isomer shift (IS) is given in mm $s^{-1}$relative to α-Fe foil. <QS> = $e^2qQ/2$ (in mm $s^{-1}$) and σ (in mm $s^{-1}$) are the average quadrupole splitting and the Gaussian width of the QS distribution of the given spectral component, respectively.

| Sample | <QS> (mm $s^{-1}$) | σ (mm $s^{-1}$) | IS (mm $s^{-1}$) | Area (%) | Site |
|---|---|---|---|---|---|
| $Fe_{1.0}$SiBEA(w) | 0.64 | 0.20 | 0.25 | 61 | $Fe^{3+}(Fe_{Td1})$ |
| | 1.01 | 0.30 | 0.25 | 39 | $Fe^{3+}(Fe_{Td2})$ |
| C-$Fe_{1.0}$SiBEA(w) | 0.66 | 0.21 | 0.22 | 32 | $Fe^{3+}(Fe_{Td1})$ |
| | 1.02 | 0.37 | 0.20 | 68 | $Fe^{3+}(Fe_{Td2})$ |

**Table 2**. The BE values (eV) of Fe 2p core excitation obtained for as prepared and calcined $Fe_{1.0}$SiBEA samples.

| Core excitation | $Fe_{1.0}$SiBEA(w) | C-$Fe_{1.0}$SiBEA(w) |
|---|---|---|
| | BE (eV) | BE (eV) |
| Fe $2p_{3/2}$ | 711.0 | 711.2 |
| Fe $2p_{1/2}$ | 724.2 | 724.2 |
| satellites | 715.0 | 715.2 |
| | 729.2 | 728.4 |

**Figure Captions**

**Figure 1.** XRD patterns recorded at ambient atmosphere of SiBEA, $Fe_{1.0}$SiBEA(p) and $Fe_{1.0}$SiBEA(w).

**Figure 2.** FTIR spectra recorded at room temperature of SiBEA and $Fe_{1.0}$SiBEA(w).

**Figure 3.** DR UV-vis spectra recorded at ambient atmosphere of $Fe_{1.0}$SiBEA(w), C-$Fe_{1.0}$SiBEA(w), $Fe_{1.0}$SiBEA(p) and C- $Fe_{1.0}$SiBEA(p).

**Figure 4.** $^{57}$Fe Mössbauer spectra recorded at room temperature of $Fe_{1.0}$SiBEA(w) and C-$Fe_{1.0}$SiBEA(w).

**Figure 5.** Si 2p XP spectra recorded at room temperature of $Fe_{1.0}$SiBEA(w) and C-$Fe_{1.0}$SiBEA(w).

**Figure 6.** O 1s XP spectra recorded at room temperature of $Fe_{1.0}$SiBEA(w) and C-$Fe_{1.0}$SiBEA(w).

**Figure 7.** Fe 2p XP spectra recorded at room temperature of $Fe_{1.0}$SiBEA(w) and C-$Fe_{1.0}$SiBEA(w).

**Figure 8.** FTIR difference spectra (OH stretching region) of $Fe_{1.0}$SiBEA(w) after adsorption of CO at 100 K: equilibrium CO pressure of 100 Pa (a) and development of the spectra during evacuation at 100 K (b–e).

**Figure 9.** FTIR difference spectra (carbonyl stretching region) of $Fe_{1.0}$SiBEA(w) after adsorption of CO at 100 K: equilibrium CO pressure of 100 Pa (a) and development of the spectra during evacuation at 100 K (b–e).

**Figure 10.** Profile of CO conversion versus temperature for C- $Fe_{1.0}$SiBEA(w), C-$Fe_{1.0}$SiBEA(p) and 1%Fe/$SiO_2$ catalysts.

**Figure 11.** BEA zeolites structure with periodical building units and with tetrahedral T1-T9 sites (based on works [60-63])

**Figure 12.** The model of the structure of $Fe_{Td1}$ non active centres located in T1 or T2 positions.

**Figure 13.** The model of the structure of active centres before (a) and after their calcination (b) as ($Fe_{Td1}$) and ($Fe_{Td2}$) centres, respectively, and after reduction (c) located in T8 position.

**Figure 14.** Profile of TPR-CO versus temperature for C-$Fe_{1.0}$SiBEA(w), C-$Fe_{1.0}$SiBEA(p) and 1%$Fe/SiO_2$

**Figure 15**. The activity of C-$Fe_{1.0}$SiBEA(w) catalyst, reduced in the mixture of 2 vol. % CO and 98 vol. % He at 473, 573, 673 and 773 K (curves 1-4 respectively), in CO oxidation (CO: air = 0.35 : 99,65 vol.%, space velocity 19100 $h^{-1}$).

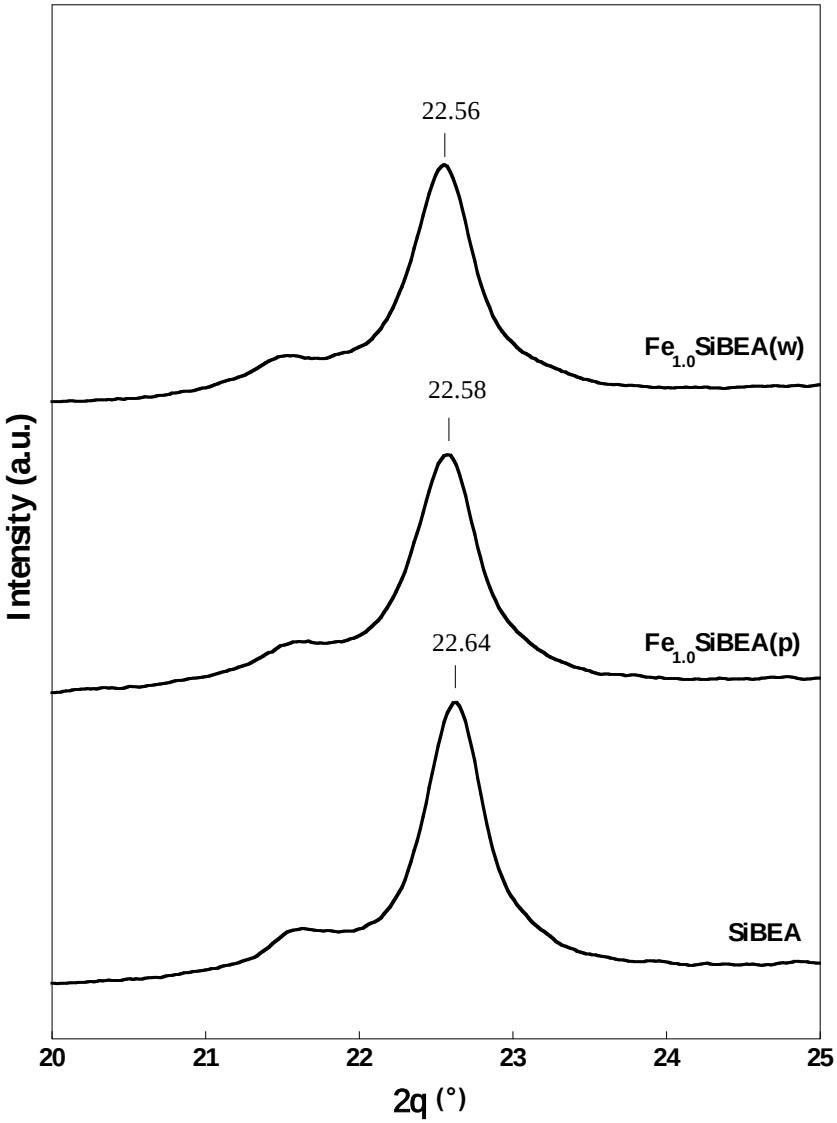
22.56
Fe1.0SiBEA(w)
22.58
Fe1.0SiBEA(p)
22.64
SiBEA
Intensity (a.u.)
20
21
22
23
24
25
2q (°)

Figure 1

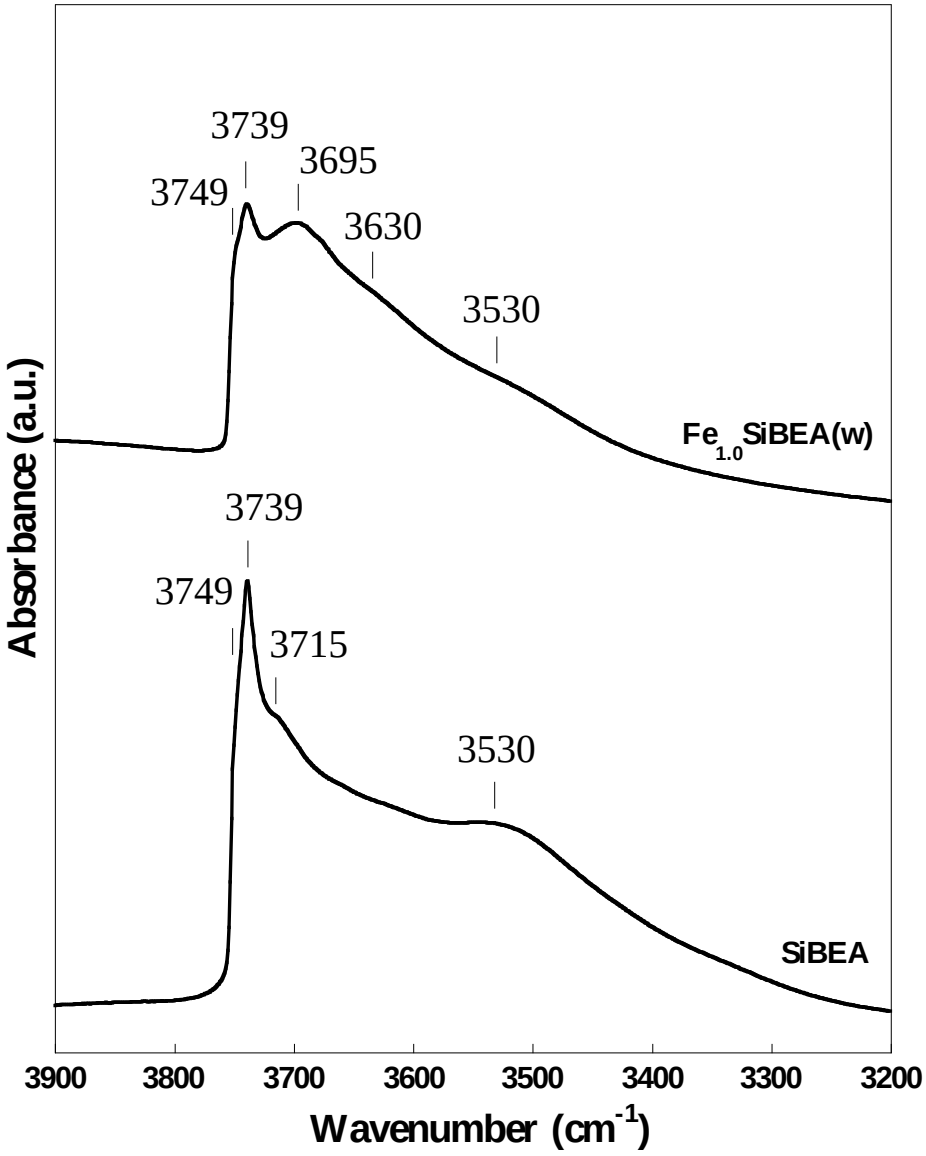
3739
3695
3749
3630
3530
Fe1.0SiBEA(w)
3739
3749
3715
3530
SiBEA
Absorbance (a.u.)
3900
3800
3700
3600
3500
3400
3300
3200
Wavenumber (cm-1)

Figure 2

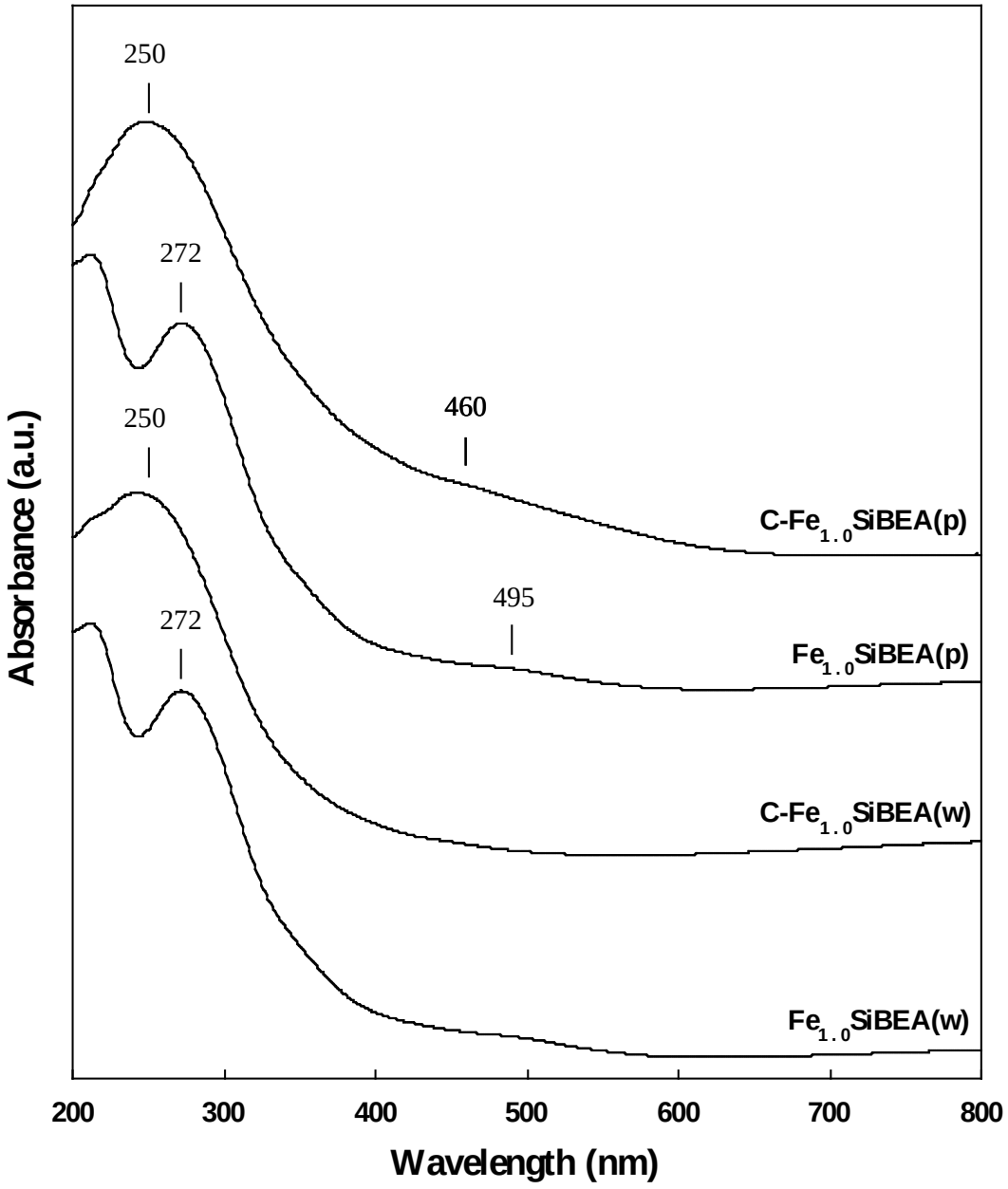
250
272
460
250
495
272
C-Fe1.0SiBEA(p)
Fe1.0SiBEA(p)
C-Fe1.0SiBEA(w)
Fe1.0SiBEA(w)
Absorbance (a.u.)
200
300
400
500
600
700
800
Wavelength (nm)

Figure 3

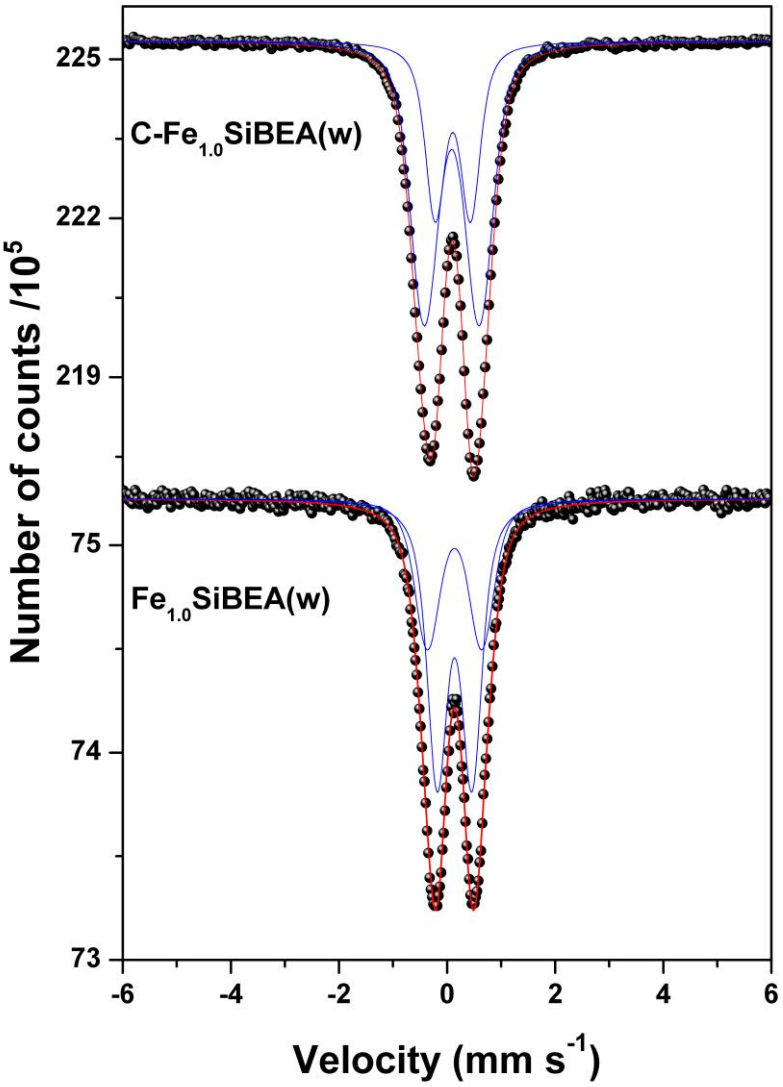
C-Fe1.0SiBEA(w)
Fe1.0SiBEA(w)
Number of counts /10^5
Velocity (mm s^-1)
225
222
219
75
74
73
-6
-4
-2
0
2
4
6

Figure 4

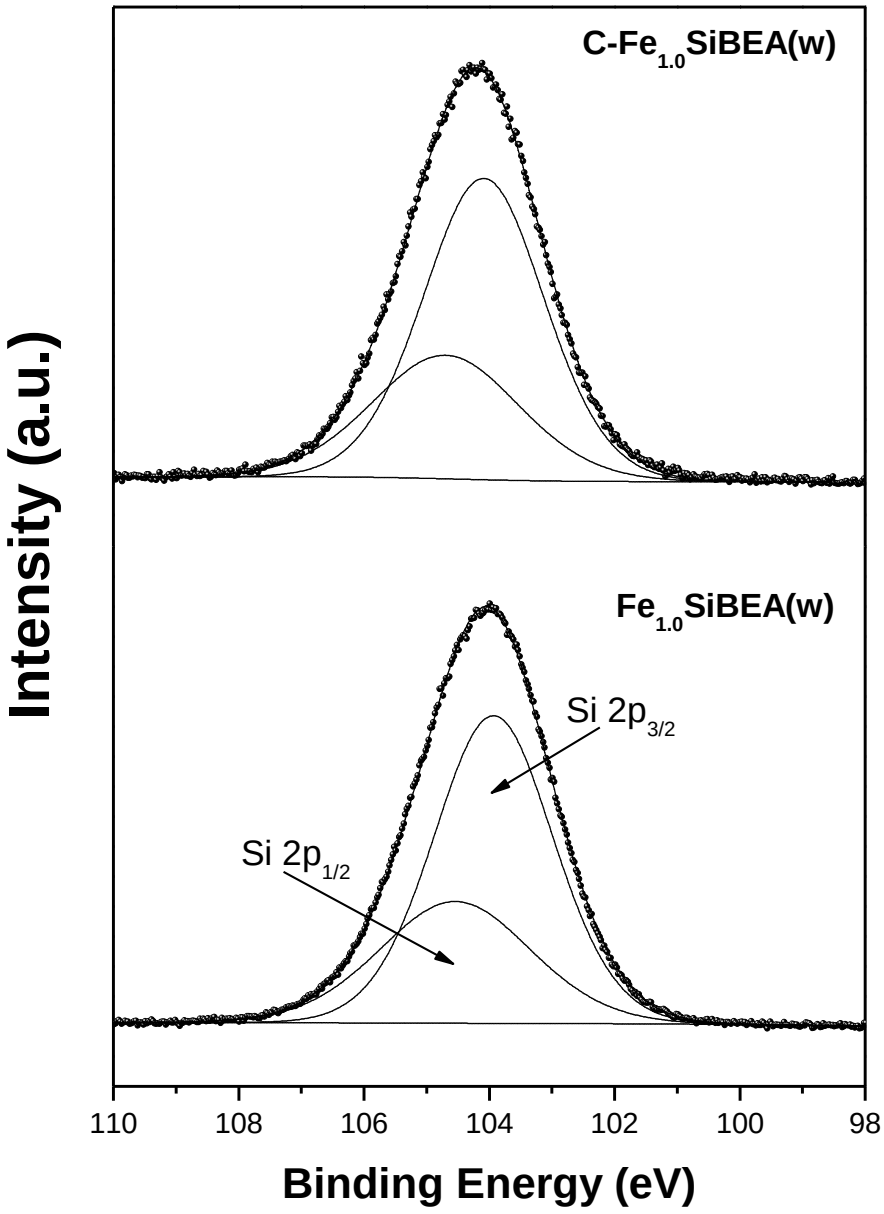
C-Fe1.0SiBEA(w)
Fe1.0SiBEA(w)
Si 2p3/2
Si 2p1/2
Intensity (a.u.)
110
108
106
104
102
100
98
Binding Energy (eV)

Figure 5

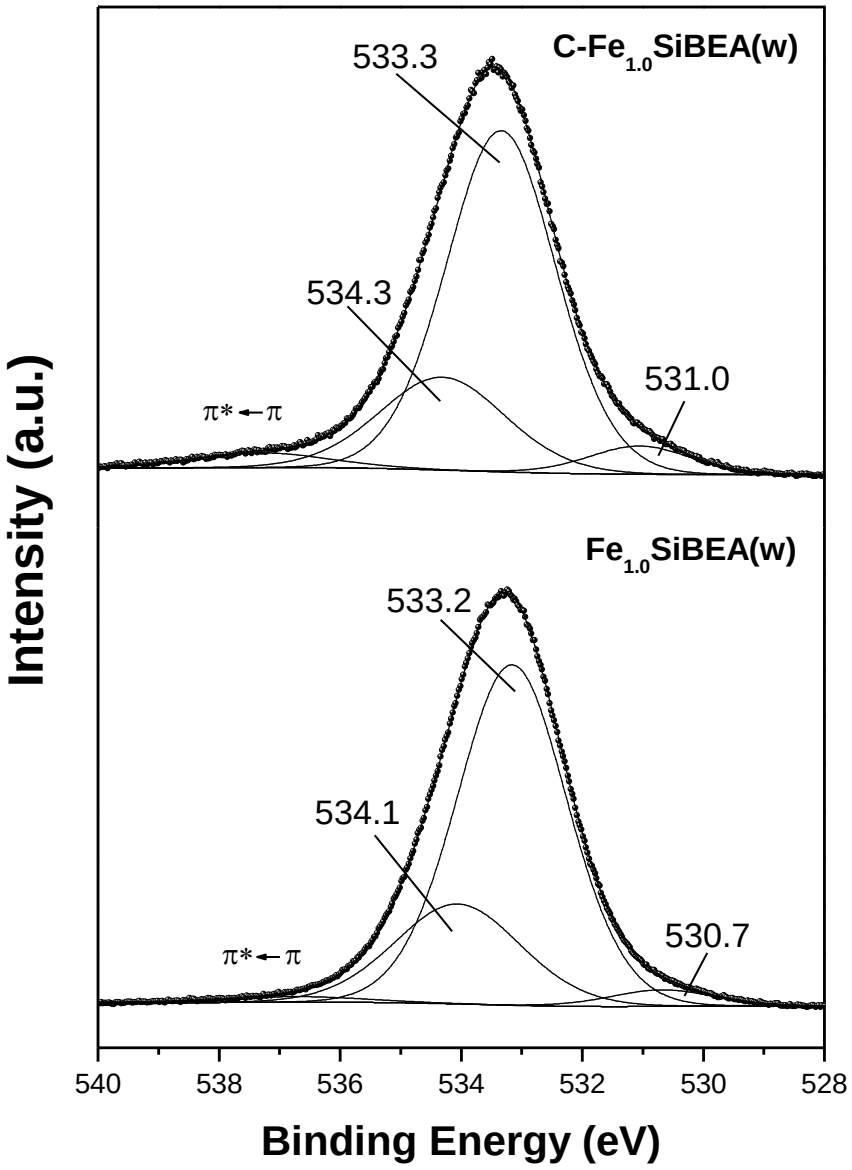
C-Fe1.0SiBEA(w)
533.3
534.3
531.0
π*←π
Fe1.0SiBEA(w)
533.2
534.1
530.7
π*←π
Intensity (a.u.)
540
538
536
534
532
530
528
Binding Energy (eV)

Figure 6

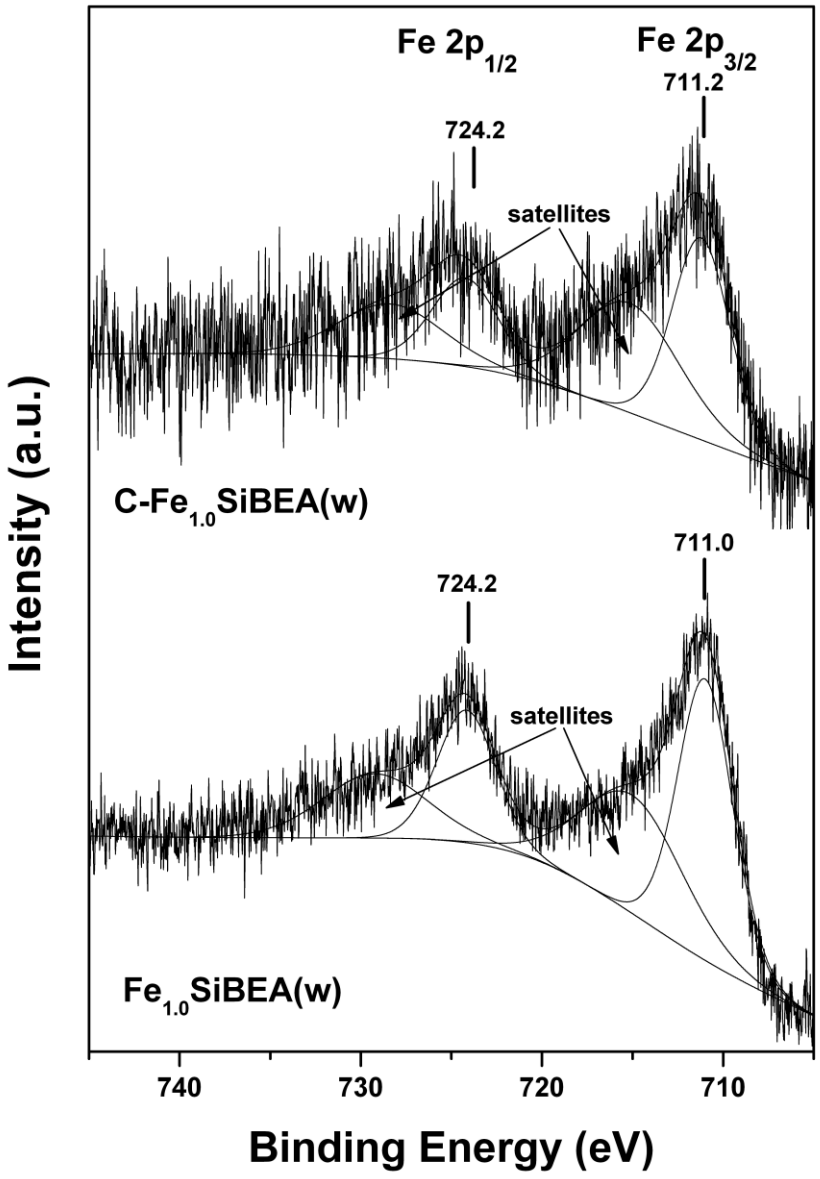
Fe 2p1/2
Fe 2p3/2
711.2
724.2
satellites
C-Fe1.0SiBEA(w)
711.0
724.2
satellites
Fe1.0SiBEA(w)
Intensity (a.u.)
740
730
720
710
Binding Energy (eV)

Figure 7

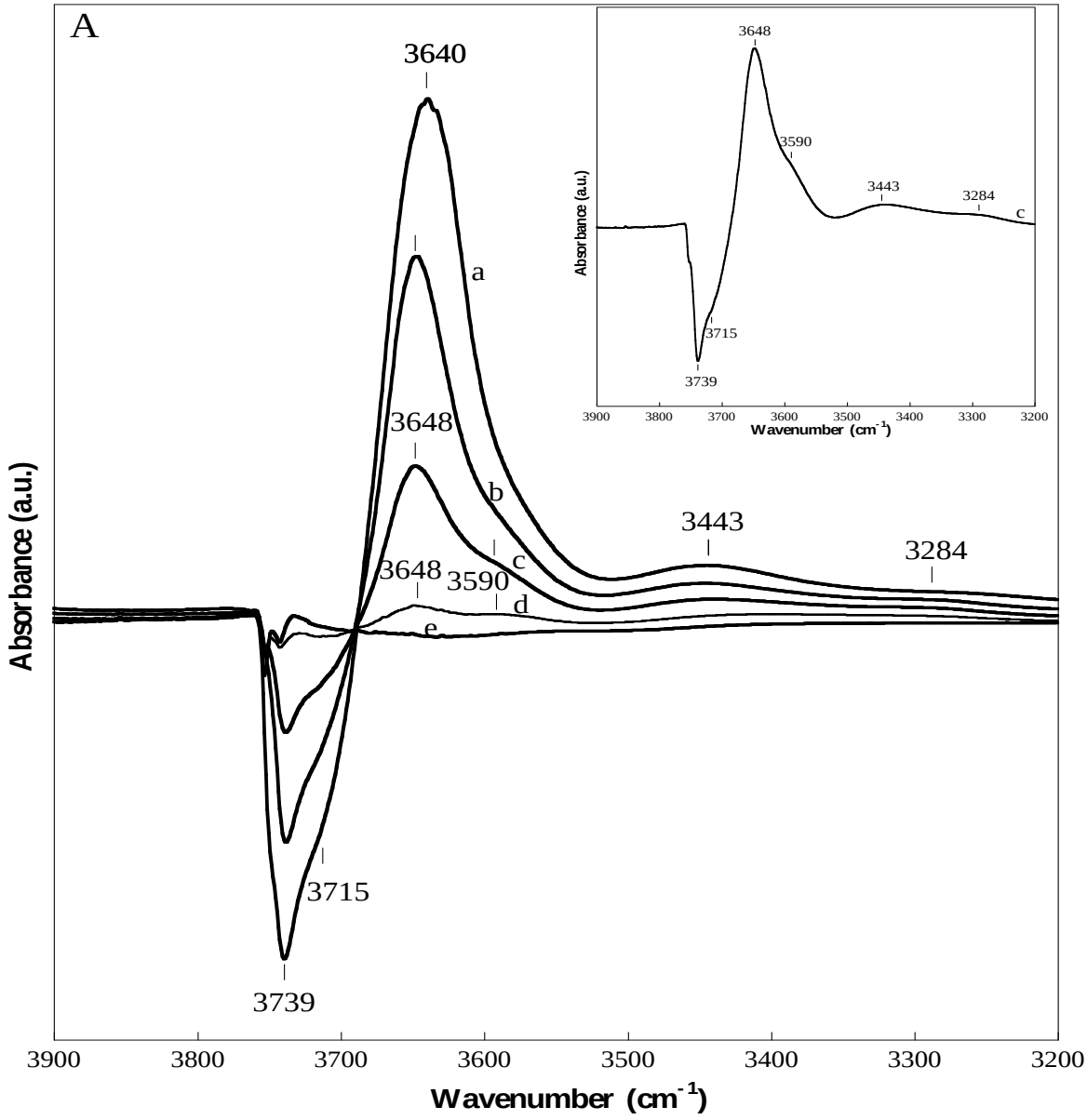
A
3640
a
3648
b
3443
3284
3648
3590
c
d
e
3715
3739
Absorbance (a.u.)
3900
3800
3700
3600
3500
3400
3300
3200
Wavenumber (cm-1)
3648
3590
3443
3284
c
3715
3739
Absorbance (a.u.)
3900
3800
3700
3600
3500
3400
3300
3200
Wavenumber (cm-1)

Figure 8

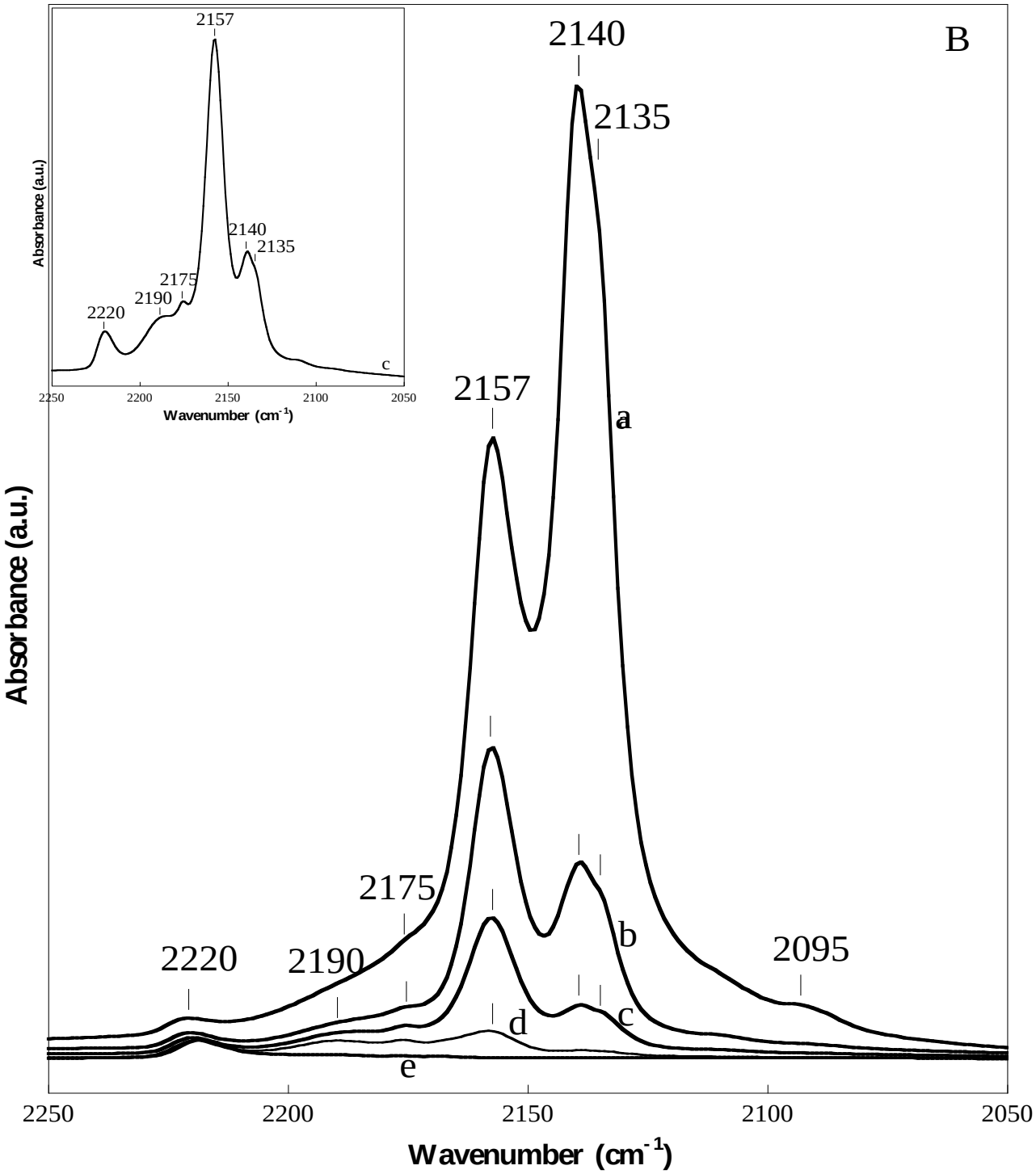
B
2140
2135
2157
a
2175
2190
2220
b
2095
c
d
e
Absorbance (a.u.)
Wavenumber (cm-1)
2250
2200
2150
2100
2050
2157
2140
2135
2175
2190
2220
c
Absorbance (a.u.)
Wavenumber (cm-1)

Figure 9

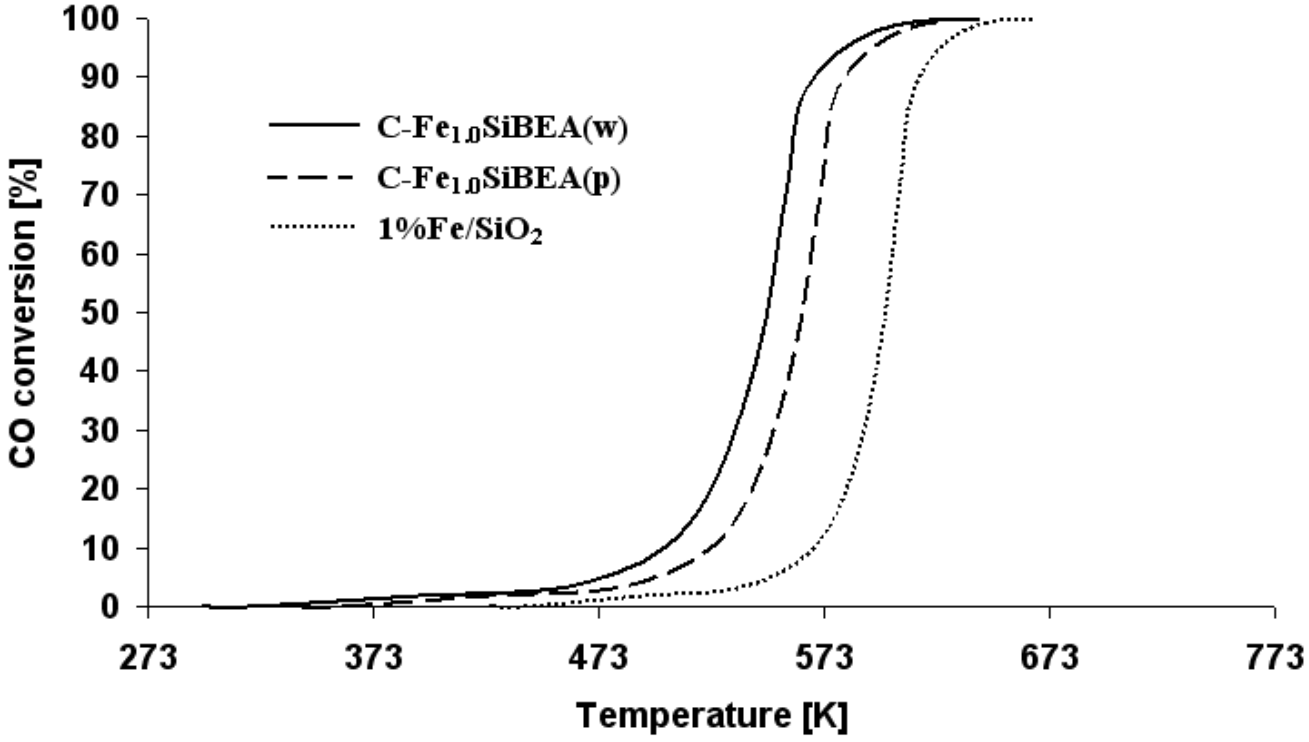
100
90
80
70
60
50
40
30
20
10
0
CO conversion [%]
C-Fe1.0SiBEA(w)
C-Fe1.0SiBEA(p)
1%Fe/SiO2
273
373
473
573
673
773
Temperature [K]

Figure 10

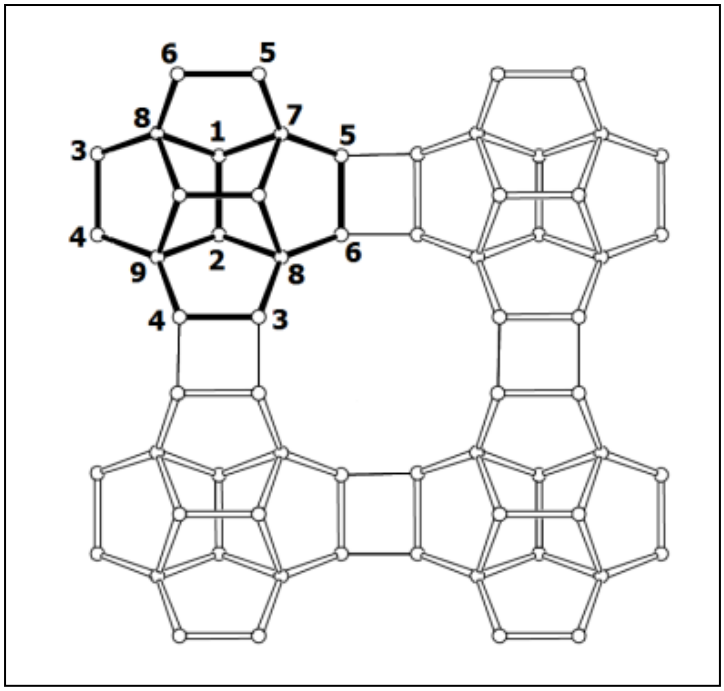


Figure 11

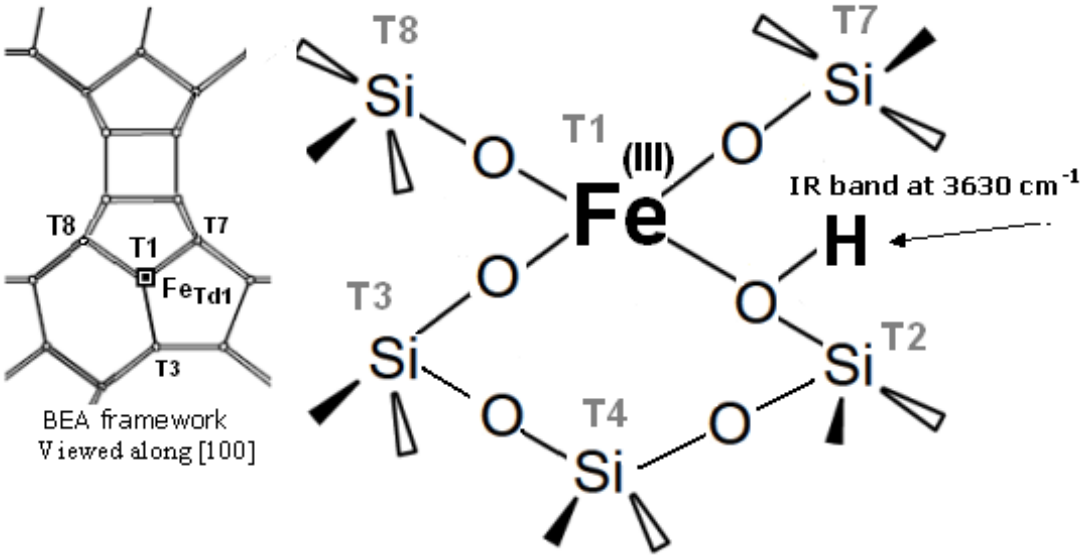
T8
T7
T1
Fe Td1
T3
BEA framework
Viewed along [100]
T8
Si
T7
Si
T1
(III)
O
O
Fe
IR band at 3630 cm-1
H
O
O
T3
Si
T2
Si
O
T4
O
Si

Figure 12

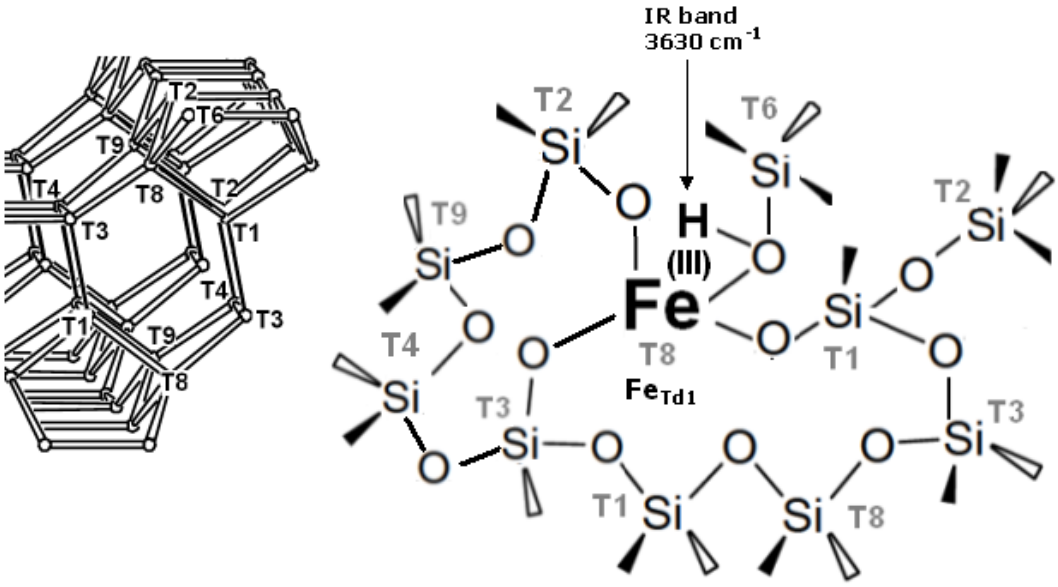
T2
T6
T9
T4
T8
T2
T3
T1
T4
T1
T9
T3
T8
IR band
3630 cm-1
T2
Si
O
T6
Si
H
(III)
O
T2
Si
T9
Si
O
Fe
O
Si
O
T4
O
T8
T1
O
Si
Fe Td1
T3
T3
Si
O
Si
O
O
O
Si
T1
Si
Si
T8

Figure 13(a)

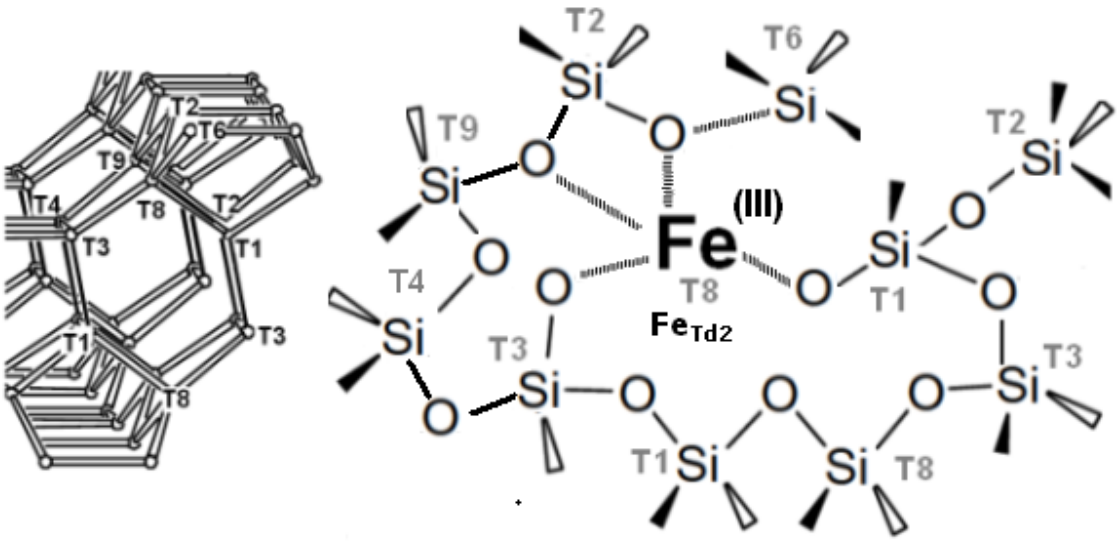
T2
T6
T9
T4
T8
T2
T3
T1
T1
T3
T8
T2
T6
T9
Si
O
Si
T2
Si
T4
O
O
Fe
(III)
O
Si
O
Si
T4
T8
T1
O
Fe Td2
T3
T3
Si
O
Si
O
O
O
Si
O
T1
Si
Si
T8

Figure 13(b)

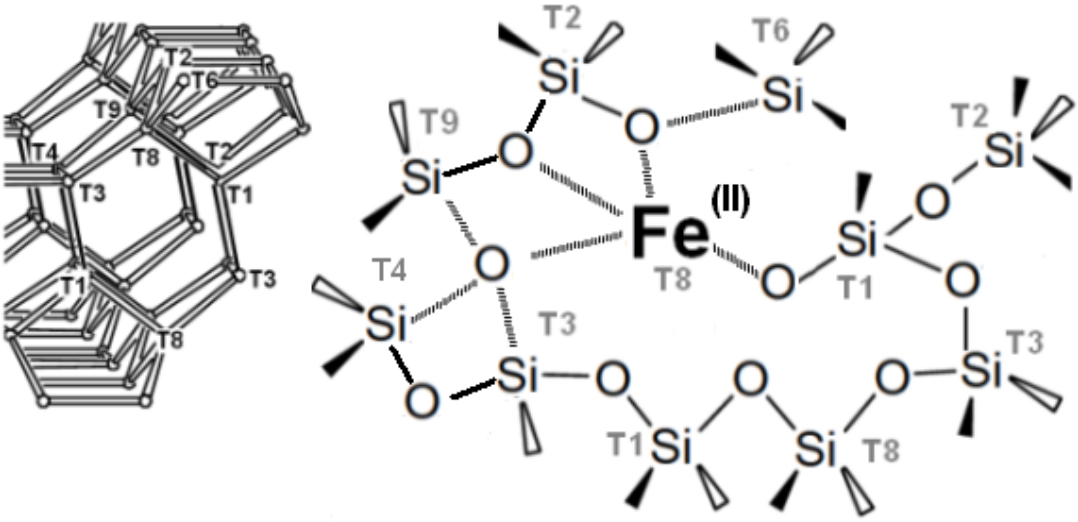
T2
T6
T9
T4
T8
T2
T3
T1
T1
T3
T8
T2
Si
T6
Si
T9
Si
O
O
T2
Si
Fe
(II)
O
Si
O
T4
O
T8
O
T1
O
Si
T3
T3
Si
O
Si
O
O
O
Si
T1
Si
Si
T8

Figure 13(c)

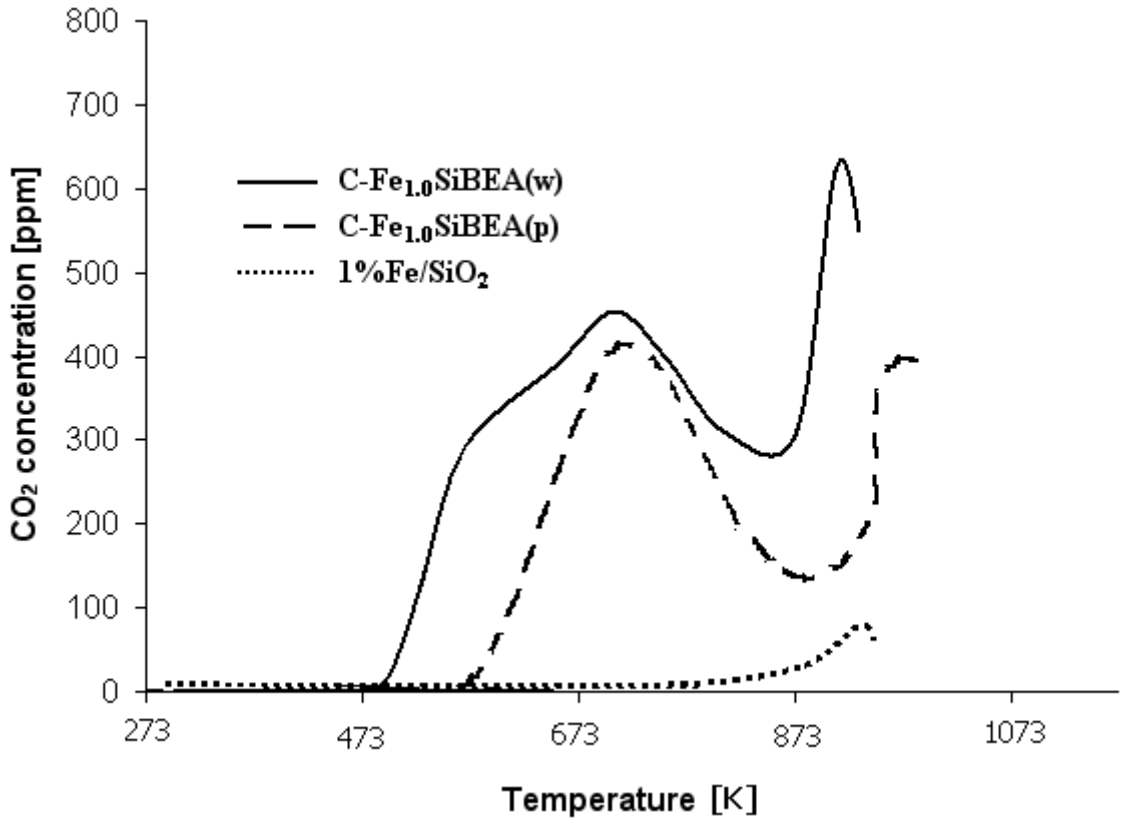
800
700
600
500
400
300
200
100
0
273
473
673
873
1073
CO2 concentration [ppm]
Temperature [K]
C-Fe1.0SiBEA(w)
C-Fe1.0SiBEA(p)
1%Fe/SiO2

Figure 14

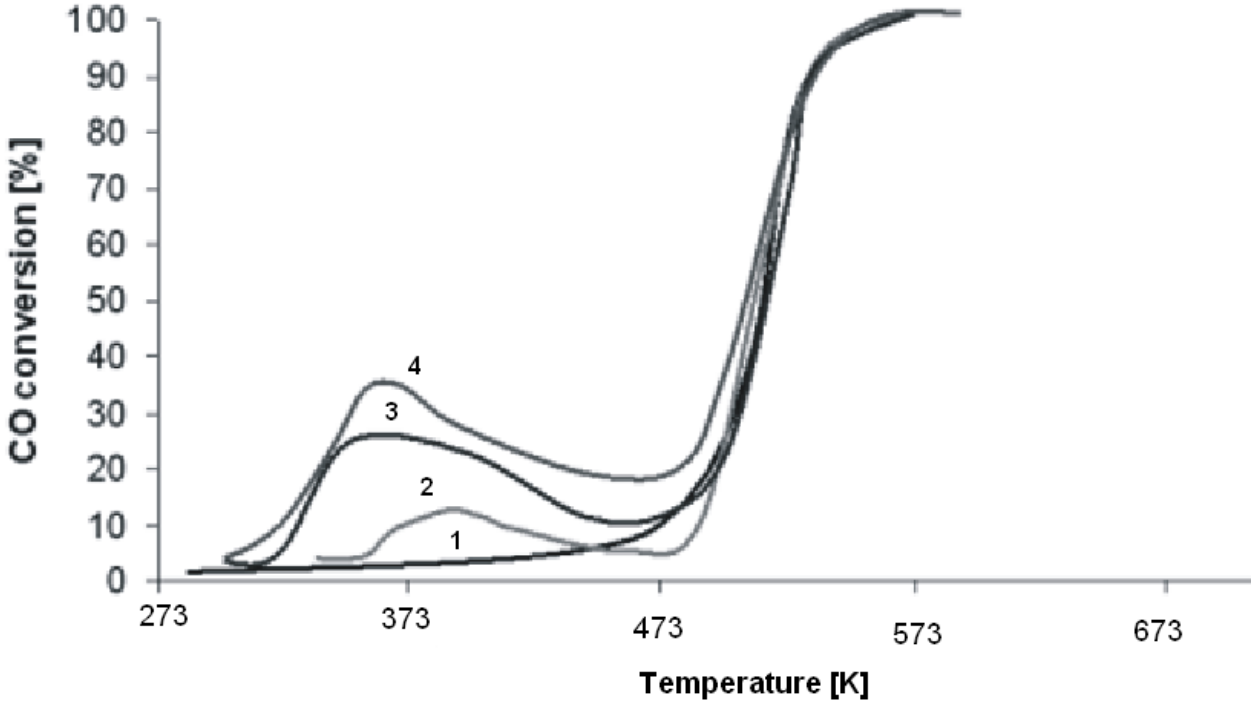
100
90
80
70
60
50
40
30
20
10
0
CO conversion [%]
4
3
2
1
273
373
473
573
673
Temperature [K]

Figure 15